VARIABILITY IN SULFUR ISOTOPE RECORDS OF PHANEROZOIC SEAWATER SULFATE

Theodore M. Present[1], Jess F. Adkins[1], and Woodward W. Fischer[1]

[1]California Institute of Technology, Pasadena, California, USA

Corresponding author: Theodore M. Present (ted@caltech.edu)

Key Points

- 6710 measurements of $\delta^{34}S$ of sulfate in Phanerozoic sedimentary rocks were compiled and systematically updated to a consistent time scale
- Records derived from evaporites, barite, and carbonate-associated sulfate are similar, but also contain dramatic short-term discrepancies
- Variation created by diagenetic and depositional processes increases with age in all records, obscuring temporal trends in marine sulfate

Plain Language Summary

Sedimentary rocks deposited in ancient marine basins preserve a record of seawater composition. We compare the sulfur isotopic composition of three sedimentary materials that contain sulfate—a major ion in seawater important for carbon and oxygen cycling. Evaporite salts, the mineral barite, and trace sulfate in limestone each reveal the same first-order trends over the last 541 million years, but also display substantial shorter order discrepancies that reflect how the materials capture and store paleooceanographic information. These discrepancies partially obscure understanding of the relationship between life, ocean chemistry, and climate.

Keywords

Phanerozoic seawater composition; marine sulfate proxies; carbonate-associated sulfate; evaporites; barite; sulfur isotope ratios; kriging

Abstract

The $\delta^{34}S$ of seawater sulfate reflects processes operating at the nexus of sulfur, carbon, and oxygen cycles. However, knowledge of past seawater sulfate $\delta^{34}S$ values must be derived from proxy materials that are impacted differently by depositional and post-depositional processes. We produced new timeseries estimates for the $\delta^{34}S$ value of seawater sulfate by combining 6710 published data from three sedimentary archives—marine barite, evaporites, and carbonate-associated sulfate—with updated age constraints on the deposits. Robust features in multiple records capture temporal trends in the $\delta^{34}S$ value of seawater and its interplay with other Phanerozoic geochemical and stratigraphic trends. However, high-frequency discordances indicate that each record is differentially prone to depositional biases and diagenetic overprints. The amount of noise, quantified from the variograms of each record, increases with age for all $\delta^{34}S$ proxies, indicating that post-depositional processes obscure detailed knowledge of seawater sulfate's $\delta^{34}S$ value deeper in time.

1 Introduction

Seawater sulfate acts as a major oxidant of organic carbon, controlling the cadence of its burial in sediments and connecting the carbon, sulfur, and oxygen cycles (Bowles et al., 2014; Jørgensen, 1982). Microbial sulfate reduction (MSR), reoxidation of sulfide, and the burial and oxidation of pyrite govern sedimentary inorganic carbon and alkalinity fluxes (Ben-Yaakov, 1973; Froelich et al., 1979). Pyrite in sedimentary rocks may be exposed and oxidized during uplift, erosion, and weathering—impacting Earth's dioxygen and carbon dioxide budgets on tectonic timescales (Burke et al., 2018; Kump & Garrels, 1986; M. A. Torres et al., 2014). Over Phanerozoic time (the past 541 Myr), the burial of sulfide and disulfide minerals must have balanced the acid produced and dioxygen consumed during terrestrial pyrite weathering. Therefore, tracking ancient sulfate fluxes related to these processes illuminates when, how, and where the Earth system achieves this balance, and what happens during intervals of unsteadiness.

Thode et al. (1953) first recognized that a record of ancient marine sulfur isotopic compositions ($\delta^{34}S$) could constrain changes to Earth's biogeochemical cycles, and Ault and Kulp (1959) applied mass balance assumptions in an early effort to quantify important sulfur fluxes. Isotope fractionations during MSR preferentially enrich the residual sulfate in ^{34}S by several percent (Bradley et al., 2016; Harrison & Thode, 1958; Sim et al., 2011). When more sulfate is reduced and fixed into pyrite, removing more light sulfur isotopes from the oceans, the remaining sulfate in seawater becomes enriched in the heavy, rare isotopes. Holland (1973) first attempted to calculate changes in dioxygen fluxes from $\delta^{34}S$ data. Holser (1977) further recognized that rapid changes in the $\delta^{34}S$ value of seawater coincide with intervals of biotic crises and dramatic reorganizations of Earth's climate and biosphere. The subsequent forty years have seen many efforts to derive an accurate and precise record of how the $\delta^{34}S$ value of seawater sulfate has changed over Earth history.

Three sedimentary materials constitute proxy archives of Phanerozoic seawater sulfate $\delta^{34}S$ values: (1) marine evaporites, which include sulfate salts precipitated from evaporated seawater in marginal marine basins; (2) marine barite, which forms from a suite of biogeochemical processes associated with sinking particles in pelagic waters; and (3) carbonate-associated sulfate (CAS), which is minor sulfate incorporated into the crystal lattice of biogenic and abiogenic calcite, aragonite, and dolomite phases that accumulate in sedimentary rocks.

Important reviews (Bottrell & Newton, 2006; Claypool et al., 1980; Holser et al., 1989; Strauss, 1997; Veizer et al., 1980) on the evolution of the Phanerozoic sulfur cycle have assumed that these proxies more-or-less accurately preserve the isotopic composition of ancient seawater sulfate. This assumption is reasonable because Phanerozoic seawater likely contained abundant sulfate as a conservative, well-mixed anion. Modern seawater has 28 mmol/kg sulfate, which has an approximate residence time of more than 10 Myr—much longer than the mixing time of the oceans (Bottrell & Newton, 2006; Walker, 1986). Supergiant gypsum and anhydrite deposits in the sedimentary record indicate that sulfate has been a major constituent in ancient seawater, as well. These deposits, which represent long-lived intervals of basin recharge and evaporation of seawater (Warren, 2010), formed episodically from Mesoproterozoic through Phanerozoic time (Grotzinger & Kasting, 1993; Pope & Grotzinger, 2003). The composition of fluid inclusions in halite from evaporite deposits further suggested that sulfate maintained at least millimolar concentrations throughout Phanerozoic time (Lowenstein et al., 2003).

Important features in the $\delta^{34}S$ age curves were observed in multiple datasets on both long and short timescales. All archives exhibited high $\delta^{34}S$ values in early Paleozoic time, fell to minima in the late Paleozoic, and increased to modern values (~21‰) over Mesozoic and Cenozoic time. This pattern was originally noted in the evaporite record by Ault and Kulp (1959) and reaffirmed by more extensive evaporite compilations (Claypool et al., 1980; Holser et al., 1989; Holser & Kaplan, 1966; Strauss, 1997). Burdett et al. (1989) produced the first continuous biogenic CAS dataset for the Neogene Period and demonstrated that it agreed with the evaporite $\delta^{34}S$ record. Kampschulte et al. (2001) and Kampschulte and Strauss (2004) then demonstrated that biogenic CAS captured the first-order features of the Phanerozoic evaporite record, and could be correlated with higher resolution and confidence than evaporites to the carbonate carbon isotope record. The $\delta^{34}S$ pattern covaries with many other geochemical records of changing seawater composition (Hannisdal & Peters, 2011; Prokoph et al., 2008), and so has been interpreted to reflect long-term changes related to the assembly and breakup of Pangea (Turchyn & DePaolo, 2019).

In addition to long-term trends, Holser (1977) identified shorter fluctuations (5–50 Myr) in the Upper Devonian and lower Triassic evaporite record; these excursions are recorded by CAS as well (Kampschulte & Strauss, 2004). Increased temporal resolution from barite and CAS found additional rapid excursions, notably associated with Jurassic and Cretaceous intervals of widespread organic-rich shale deposition (Gill, Lyons, & Jenkyns, 2011; Paytan et al., 2004) and Paleogene carbon cycle perturbation (Paytan et al., 1998; Rennie et al.,

2018). In addition, some $\delta^{34}S$ records with high temporal resolution, especially derived from CAS, have rapid variability (Kah et al., 2016; Kampschulte et al., 2001), and data from multiple locations containing similar-age strata have $\delta^{34}S$ heterogeneity (Gill, Lyons, Young, et al., 2011; Present et al., 2015).

Although seawater sulfate was likely well-mixed for much of Phanerozoic time, these rapidly varying datasets indicated that short periods of sulfate drawdown may have been expressed as high spatial and temporal $\delta^{34}S$ gradients (Holser, 1977; Kah et al., 2004, 2016). If these gradients represent globally relevant budgets of carbon, nutrients, and oxidizing capacity, then the residence time of sulfate in ancient oceans must have been much shorter than today. An analogy to the carbon cycle is illustrative. Isotopic fractionations between oxidized and reduced species are comparable for carbon and sulfur. The biological pump—remineralization of sinking organic matter that is fractionated by tens of permille from dissolved inorganic carbon—is only capable of creating inorganic carbon isotopic gradients of less than 3‰ given Pliocene-age to present nutrient inventories and *ca.* 2 mmol/kg bicarbonate (Toggweiler & Sarmiento, 1985). Therefore, even small gradients in the $\delta^{34}S$ of marine sulfate, of similar magnitude to carbon isotope gradients driven by the biological pump, would have required both a higher proportion of anaerobic organic carbon remineralization and more than an order of magnitude smaller sulfate inventory.

However, the implicit assumption that proxies for seawater $\delta^{34}S$ values are suitably accurate and precise to demonstrate rapid changes in seawater's composition has not been tested. The processes by which the proxy materials form and incorporate sulfate from seawater may affect their $\delta^{34}S$ value, complicating the reconstruction of Phanerozoic seawater's composition but providing nuance on biogeochemical sulfur cycling and its imprint on the rock record.

We produced a new timeseries to estimate the Phanerozoic history of the $\delta^{34}S$ value of seawater sulfate by synthesizing published geochemical data with updated geochronology and stratigraphic correlations. We attribute some of the differences between archives to mechanics of how sulfate is incorporated into and preserved in sedimentary rocks. This approach tests the assumption that each archive samples the same history of seawater $\delta^{34}S$ values, quantifies uncertainty in proxy archives, and reveals that some major sources of variance are themselves produced by biogeochemical processes that may have varied through Phanerozoic time.

2 Synthesis of Phanerozoic seawater sulfate $\delta^{34}S$ proxy data

We compiled 6710 measurements from 108 references that reported $\delta^{34}S$ values in Phanerozoic marine evaporites, bulk rock CAS, biogenic CAS, or marine barite. Each $\delta^{34}S$ value was assigned an age using the International Commission on Stratigraphy 2016/04 time scale (Cohen et al., 2013; updated) (Figure 1). The Supporting Information enumerates the $\delta^{34}S$ data, assigned age, data type, data source, and method and literature used for each age assignment.

Each proxy material has different, irregularly spaced temporal distributions (Figure 1a). To estimate Phanerozoic $\delta^{34}S$ trends, each proxy record was interpolated at 50 kyr resolution (Figure 1b). Kriging—a geostatistical approach using autocorrelation to quantify stochastic components in spatiotemporal data—was used to weight data for interpolation and estimate confidence intervals (Gebbers, 2010). Because kriging uses the empirical autocorrelation structure of the data to produce weights, it is well suited for irregularly spaced data. Autocorrelation varies between two endmembers of linearly detrended variance: at the maximum is the variance of all points in that geologic interval, and at the minimum is the unresolved chatter between data closely spaced in time. The kriged uncertainty on the interpolations reflects this increase in variance, such that interpolated values further from data have larger uncertainties up to the population variance according to the observed range of autocorrelation. Kriging was done on each geologic material, partitioned by era, by modelling variograms—functions describing how the variance per point (semivariance) of pairs of linearly detrended data varies with their average separation distance in time (Supporting Information). Paleogeography was not considered, so spatial variability was collapsed into the temporally unresolved chatter within each era.

Figure 1 ***[next page]*****.** Records of Phanerozoic seawater sulfate $\delta^{34}S$ generated from proxy materials. **(a)** The average number of $\delta^{34}S$ analyses of each proxy per Myr, in 5 Myr bins, illustrates the temporal bias in the sampling of each material through Phanerozoic time. **(b)** Interpolated proxy records of the $\delta^{34}S$ composition of sulfate over Phanerozoic time. Shading indicates the kriged 1σ confidence intervals. **(c)** All compiled proxy data for the $\delta^{34}S$ of Phanerozoic seawater.

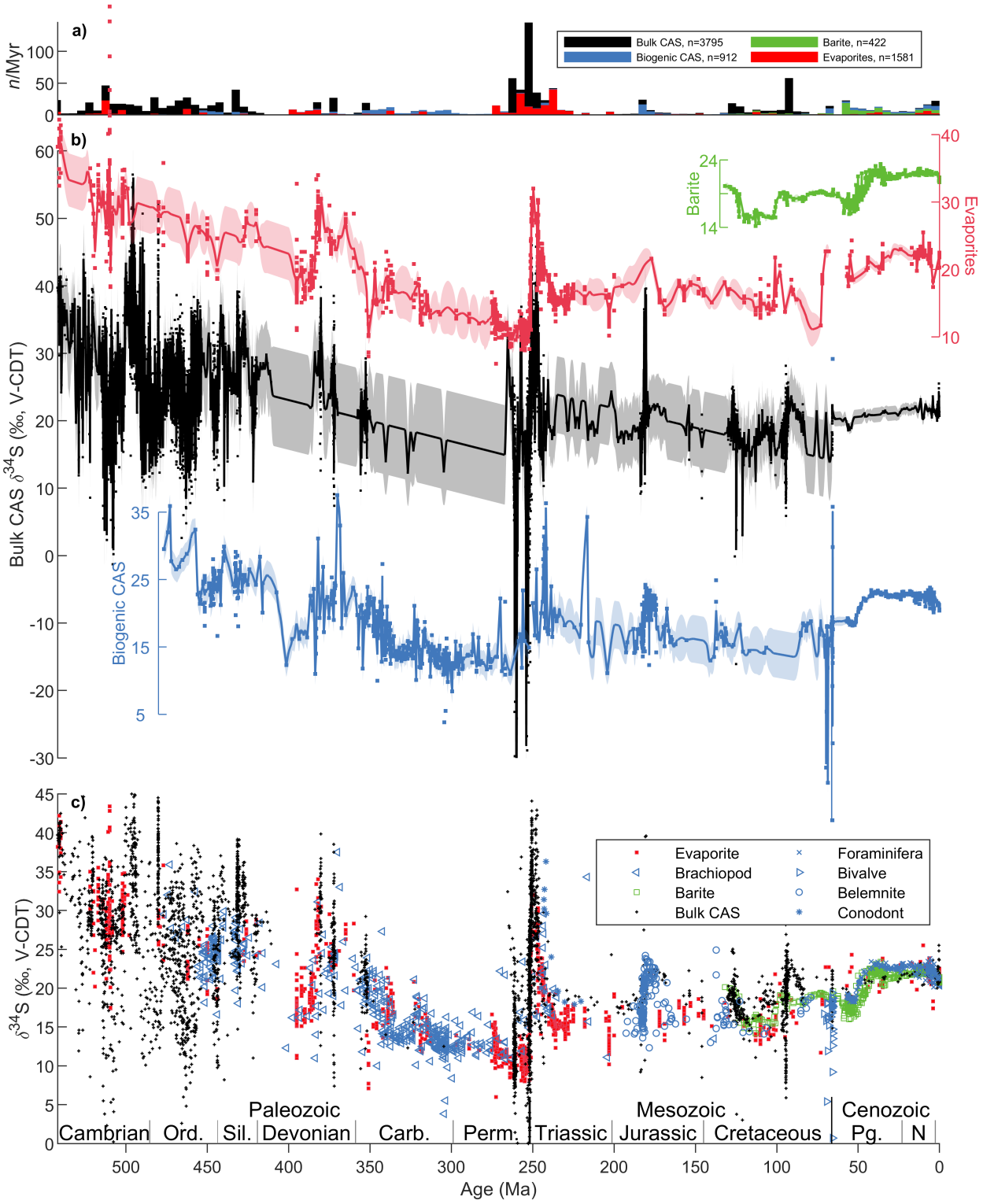
a)
n/Myr
Bulk CAS, n=3795
Biogenic CAS, n=912
Barite, n=422
Evaporites, n=1581
b)
Bulk CAS δ^{34}S (‰, V-CDT)
Barite
Evaporites
Biogenic CAS
c)
δ^{34}S (‰, V-CDT)
Evaporite
Brachiopod
Barite
Bulk CAS
Foraminifera
Bivalve
Belemnite
Conodont
Paleozoic
Mesozoic
Cenozoic
Cambrian
Ord.
Sil.
Devonian
Carb.
Perm.
Triassic
Jurassic
Cretaceous
Pg.
N
Age (Ma)

3 Discussion

3.1 Distribution of $\delta^{34}S$ in proxies

During seventy years of effort to determine a history of Phanerozoic seawater sulfate $\delta^{34}S$ from different geologic materials, it has implicitly been assumed that each proxy samples the same primary population of seawater $\delta^{34}S$ compositions through space and time. However, comparison of all Phanerozoic $\delta^{34}S$ data for each proxy indicates that the four datasets do not come from the same distribution (Supporting Information, non-parametric Kruskal-Wallis one-way analysis of variance, $\chi^2[3,6709] = 684.54$, $p \ll 0.001$). Therefore, each proxy likely has different temporally or spatially variable sampling biases or reflects different biogeochemical processes that contribute to variance in the time-series of ancient sulfate's $\delta^{34}S$.

Major $\delta^{34}S$ trends and excursions in Cenozoic, Mesozoic, and late Paleozoic records are exhibited in multiple archives, but significant discrepancies and gaps are apparent in records from Cambrian to Devonian time (Figure 1c). In early- to mid-Paleozoic strata, biogenic carbonates are sparse, marine barite is absent, and bulk CAS $\delta^{34}S$ values diverge from evaporites by greater than 10‰ (Figure 2a). Additionally, Paleozoic variance is highest for all records (Figure 2b).

The evaporite record, being comprised of massive amounts of sulfate but limited in spatial and temporal extent, likely captures long-term $\delta^{34}S$ trends. The bulk CAS, biogenic CAS, and barite records have higher temporal resolution than the evaporite record for much of the Phanerozoic, potentially capturing shorter $\delta^{34}S$ excursions.

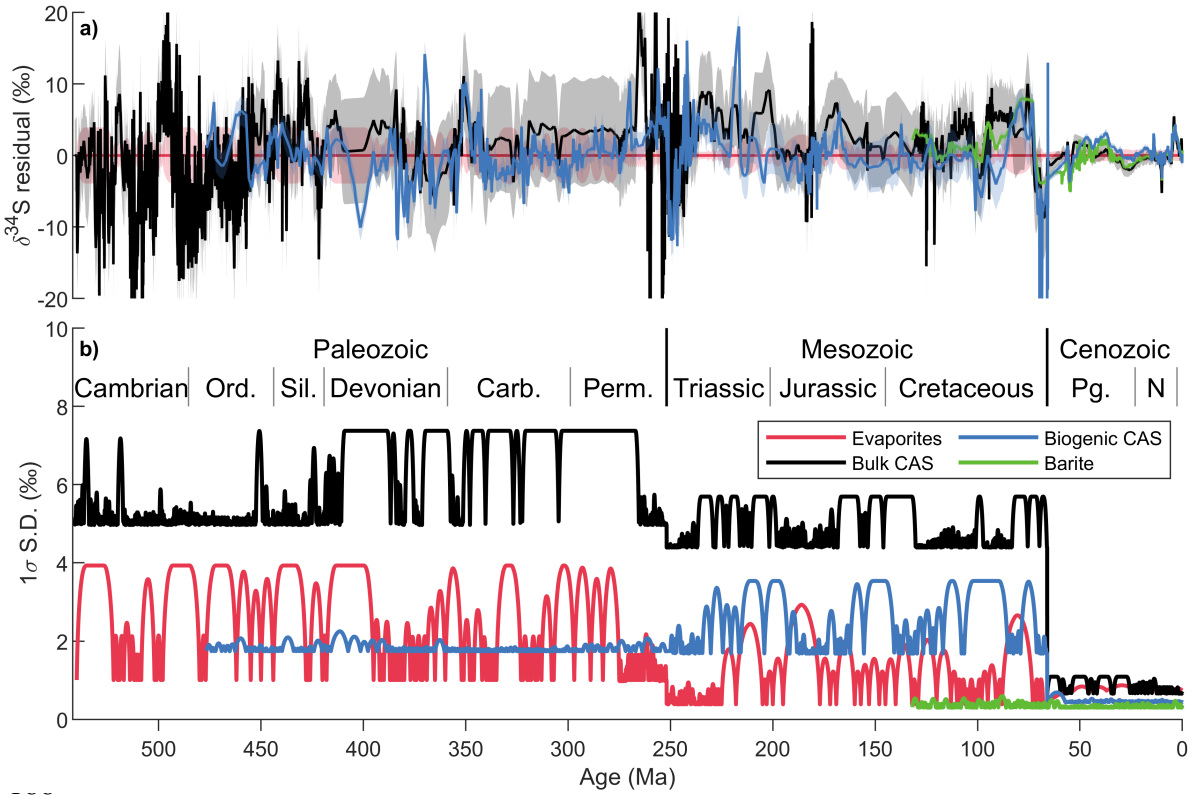

Figure 2. Comparison of $\delta^{34}S$ values and variance generated from proxy materials. **(a)** Residuals between the evaporite record and each other record shaded with kriged 1σ confidence intervals. **(b)** Confidence intervals produced from kriging data from each proxy in each era. Where data is sparse, the confidence intervals approach the standard deviation of linearly detrended data in each geologic era, excluding 1st and 99th percentile outliers. Where there is data, the confidence interval is the uncorrelated chatter determined from the semivariance of data temporally closer than the mean minimum time between data pairs.

3.2 Sources of $\delta^{34}S$ variance

The $\delta^{34}S$ variability for each proxy is plotted in Figure 2b. The maxima in each era on each curve represents the standard deviation of detrended $\delta^{34}S$ data over each geologic era. For example, the standard deviation of linearly detrended Paleozoic bulk CAS data is 7.4‰ (excluding 1st and 99th percentile outliers), while that of all Cenozoic barite data is 1.3‰. These standard deviations can be interpreted as a naive description of expected variability where data is sparse, and reflect the combination of local spatiotemporal trends in the proxy record plus an uncorrelated random component. The uncorrelated, random component is estimated by the semivariance of pairs of data that are closer together than the mean

minimum time between all pairs of data (Gebbers, 2010). The uncorrelated variances for each proxy are plotted as the minima in each era on each curve in Figure 2b.

Uncorrelated variance is a metric that convolves multiple sources of uncertainty. Sources of variance of geologic interest include temporally unresolved variability in seawater $\delta^{34}S$ values and temporally incoherent variability in how the sedimentary archives were formed or altered. These sources of variance may be temporally unresolved due either to spatial variability of seawater sulfate's $\delta^{34}S$ at a given time, or to temporal variability more rapid than the resolution of the record. In addition, the uncorrelated variance captures analytical uncertainty related to making $\delta^{34}S$ measurements in each archive, and non-systematic error in age assignments of proxy materials. While the relative contributions of each of these sources of uncertainty may differ between proxies or with age, the uncorrelated variance metric—like the population variance—describes the data's structure and how predictive a given $\delta^{34}S$ measurement is of other nearby values.

This analysis produced two key results: the uncorrelated variance is different for each archive, and for all archives it increases with age. Cenozoic and Mesozoic CAS data have uncorrelated variance larger than that of evaporites and barite. Uncorrelated Paleozoic bulk rock CAS data have a standard deviation more than twice that of biogenic CAS and evaporites. Differences between multiple proxies of the same age indicate that the uncorrelated variance is likely caused, in part, by variability inherent to how $\delta^{34}S$ is preserved, rather than just inadequate sampling of primary spatial and temporal variability of seawater sulfate.

The remaining analysis considers the sources of variance in each archive that may have contributed to the uncorrelated variance. Importantly, trends statistically distinguishable from the uncorrelated variance need not represent true trends in the $\delta^{34}S$ of Phanerozoic seawater. The same sources of variance controlling the uncorrelated data may themselves have spatial or temporal components that lead to biased estimates of Phanerozoic seawater's composition in the proxy records. The uncorrelated variance, in part, quantifies the disagreement between contemporaneous records from different localities. Trends in the data smaller than the uncorrelated variance are indistinguishable from random noise. This is true even for individual records from stratigraphic successions with coherent $\delta^{34}S$ trends: a given stratigraphic succession may clearly resolve a trend in the $\delta^{34}S$ of the proxy but fail to statistically resolve a global trend in the $\delta^{34}S$ of seawater sulfate.

3.2.1 Evaporites

Deposits of carbonate, sulfate, and halide salts form as seawater evaporates in restricted basins. Throughout Phanerozoic time, bedded marine evaporites formed subaqueously, in salinas (hypersaline lagoons) and salt pans, and subaerially, in supratidal sabkha environments. Extremely thick (>100s of meters) evaporite deposits have also formed in deeper-water environments. Deposition and preservation of evaporites require favorable climatic and tectonic conditions where restricted basins experience net evaporation (Warren,

2010). Therefore, the evaporite record has limited spatial and temporal continuity (Claypool et al., 1980; Strauss, 1997).

Because evaporites are massive products of seawater sulfate, they are largely expected to provide an accurate proxy for the $\delta^{34}S$ of ancient seawater sulfate. However, because they form in marginal marine environments often with biologically adverse salinities, it can be difficult to constrain their geologic age with biostratigraphy. In many deposits, it is also challenging to discern depositional environment or deconvolve marine and non-marine geochemical signatures (Hardie, 1984; Kendall & Harwood, 1989; Lu & Meyers, 2003). The restricted, marginal marine settings in which many evaporites form are prone to changes in fluid source or depositional environment with minor base-level changes (Playà et al., 2007). Basins rich in evaporites also often form diapirs that drive salt tectonics, which complicates a deposit's internal stratigraphy (Nielsen, 1989).

Evaporites can have a $\delta^{34}S$ range of 1‰ to 6‰ within a formation (Thode & Monster, 1965). This variability cannot be attributed to fractionation during gypsum precipitation, which produces sulfate salt prior to halite saturation that has a $\delta^{34}S$ composition 1‰ to 2‰ higher than the unevaporated seawater (Raab & Spiro, 1991). Salinity stratification in evaporating basins can promote water-column anoxia and allows MSR to distill sulfate to higher $\delta^{34}S$ compositions than the original seawater; in some cases, evaporite $\delta^{34}S$ compositions are higher than other proxies from the same depositional basin (Fike & Grotzinger, 2010). Consequently, early workers hypothesized that the isotopic composition of ancient seawater was best reflected by the lowest $\delta^{34}S$ value in an evaporite succession (Ault & Kulp, 1959; Davies & Krouse, 1975; Thode & Monster, 1965). However, evaporite basins in marginal marine environments are recharged not only by unadulterated seawater, but also by groundwater and runoff with $\delta^{34}S$ compositions biased either higher or lower than seawater from remobilized older evaporite deposits or weathered sedimentary pyrite and organic sulfur (Nielsen & Ricke, 1964; Utrilla et al., 1992). Finally, high organic carbon concentrations in many evaporite deposits can promote isotope fractionation by thermochemical sulfate reduction during burial diagenesis (Vinogradov, 2007).

Some of the uncorrelated variance in evaporite isotope ratio data also results from poor stratigraphic control (Supporting Information). Here we used updated stratigraphic information to better constrain the age of evaporite data, but the record can further benefit from higher-resolution sample collection with improved stratigraphic control during intervals where $\delta^{34}S$ changes appear in other records. Modern stratigraphic models permit correlation of evaporitic strata to better-constrained carbonate and clastic strata. Bernasconi et al. (2017) recently produced a high-resolution evaporite record that resolved the major early Triassic $\delta^{34}S$ excursions seen in earlier datasets; thus careful correlation and assignment of geologic ages permits tracking changes in the Phanerozoic sulfur cycle with evaporites. Indeed, the stratigraphic control for Mesozoic evaporites provided by Bernasconi et al. (2017) likely drives the low standard deviation of uncorrelated Mesozoic evaporite data to values (0.4‰) comparable to that of the marine barite record (0.3‰).

3.2.2 Barite

Barite precipitates from hydrothermal fluids, sediment pore fluids, and from particles within the marine water column (Paytan et al., 1993, 2002). Barite is under-saturated in most of the oceans (Chow & Goldberg, 1960; Church & Wolgemuth, 1972). However, barite has been observed in sediment traps in the upper 200 m in the water column, especially in high-productivity regions, and is associated with sulfate enrichment from decaying organic matter (Bishop, 1988). While barite super-saturation is achieved predominately by the addition of sulfate from oxidizing organic sulfur (Horner et al., 2017; Jacquet et al., 2007), marine barite apparently precipitates with $\delta^{34}S$ values within 0.4‰ of modern seawater (Paytan et al., 1998, 2002). Barite is subsequently transported to sediments by fecal pellets and marine snow (Bishop, 1988), and preserved in oxic marine sediments in high-productivity regions where enough barite is delivered to saturate pore fluids (Church & Wolgemuth, 1972). Sulfate reduction in anoxic sediments can cause dissolution of barite, which re-precipitates at the base of the sulfate reduction zone with extremely high $\delta^{34}S$ compositions (M. E. Torres et al., 1996).

Marine barite is considered an accurate proxy for ancient seawater $\delta^{34}S$ because it precipitates in the open-ocean water column and is texturally distinguishable from diagenetic barite that forms in anoxic sediments at redox fronts (Paytan et al., 1993). However, the marine barite record is limited by the availability of open-marine sediments that deposited in high-productivity regions where both authigenic enrichment of barite occurs and pore fluid sulfate concentrations remain above zero (Paytan et al., 1993). Consequently, the barite $\delta^{34}S$ record is unlikely to be extended much further than the current dataset spanning the last 130 Myr. Bedded barite deposits are associated with economically-important disulfide mineral deposits (C. A. Johnson et al., 2009), but contain large $\delta^{34}S$ variability (>10‰) and do not resolve the ancient seawater record any better than other proxy materials. Additionally, with few exceptions (e.g., Yao et al., 2018), the temporal resolution of the marine barite $\delta^{34}S$ record is unlikely to dramatically improve, especially during biogeochemical events characterized by low marine productivity (such as the Cretaceous-Paleogene boundary) or bottom-water anoxia (such as ocean anoxic events) that would have limited authigenic barite enrichment or preservation.

3.2.3 Carbonate-associated sulfate

Limestones and dolomites deposited continuously throughout Phanerozoic time, accumulating in marginal marine and open-ocean environments. A minor amount of sulfate is incorporated into biogenic and abiogenic carbonate phases. Biogenic carbonates often contain part-per-thousand sulfate by mass, while inorganic cements typically contain hundreds of parts-per-million (Barkan et al., 2020; Busenberg & Plummer, 1985; Giri & Swart, 2019; Paris, Fehrenbacher, et al., 2014; Staudt & Schoonen, 1995). Recent sediments from various peritidal carbonate platform environments include CAS with an isotopic composition similar to modern seawater (Lyons et al., 2004). CAS, therefore, complements

and exceeds the temporal resolution and completeness of the evaporite and barite records (Strauss, 1997).

Diagenetic processes may exchange sulfate with the primary carbonate and alter its isotopic composition (Fichtner et al., 2017; Murray et al., 2020; Present et al., 2015, 2019). Kampschulte & Strauss (2004) suggested that the variability of multiple $\delta^{34}S$ analyses from contemporaneous stratigraphic successions could be used to quantify the effect of diagenesis on the CAS record. However, rapidly-changing and disparate CAS $\delta^{34}S$ compositions have since been generated and interpreted—especially in Paleozoic studies—as intervals of heterogeneous seawater sulfate $\delta^{34}S$ reflecting periods of low sulfate concentrations and low marine sulfate residence times (e.g., Gill, Lyons, Young, et al., 2011; Kah et al., 2004).

Limestones and dolomites are comprised of mud or grains that precipitated both biologically and abiotically from seawater, with cements binding them together. Each of these components may recrystallize in pore fluids whose chemical composition reflects marine, meteoric, and burial diagenetic processes. A combustion CAS analysis typically requires 10 g to 100 g of carbonate (Wotte et al., 2012), and this mass requirement dictates that samples mix components that may have precipitated and/or recrystallized at different times. Further, CAS analyses may be contaminated by sulfur from co-occurring phases, including sulfide and disulfide minerals, sulfur-bearing organic material, and sulfate salts (Edwards et al., 2019; Marenco, Corsetti, Hammond, et al., 2008; Present et al., 2015; Theiling & Coleman, 2015; Wotte et al., 2012). Recent application of plasma-source mass spectrometry for sulfur isotope analysis has permitted $\delta^{34}S$ analyses on less than one-thousandth as much sulfate, corresponding to 5 mg to 50 mg of carbonate (Paris, Adkins, et al., 2014; Paris et al., 2013; Present et al., 2015, 2019; Rennie et al., 2018). Well-preserved biogenic grains, recrystallized grains, matrix, and cements contain CAS with $\delta^{34}S$ compositions varying by as much as 25‰, spanning most of range of CAS analyses from the entire Phanerozoic (Present et al., 2015, 2019). Therefore, much of the variability of CAS $\delta^{34}S$ data may not reflect the $\delta^{34}S$ composition of ancient seawater sulfate. Identifying components that retain the $\delta^{34}S$ of sulfate incorporated from syndepositional seawater is critical to precisely and accurately exploit the CAS $\delta^{34}S$ archive.

CAS can reflect the $\delta^{34}S$ of syndepositional seawater sulfate if the carbonate component did not recrystallize after precipitation, if recrystallization and cementation occurred in contact with a low-sulfate fluid, or if the $\delta^{34}S$ of pore fluid sulfate was not fractionated from seawater (Gill et al., 2008; Lyons et al., 2004; Rennie & Turchyn, 2014). Alteration occurs if the sediments recrystallize above the depth at which sulfate is completely consumed by MSR but deep enough that some distillation of $\delta^{34}S$ within sediment pore fluid has occurred (Edwards et al., 2019; Fike et al., 2015; Present et al., 2019; Rennie & Turchyn, 2014; Witts et al., 2018). Additionally, some ancient carbonates contain CAS with anomalously low $\delta^{34}S$ interpreted to result from the incorporation of sulfate from sulfide that was reoxidized during diagenesis or weathering (Baldermann et al., 2015; Edwards et al., 2019; Fichtner et al., 2017; Fike et al., 2015; Marenco, Corsetti, Kaufman, et al., 2008; Present et al., 2015, 2019; Rennie & Turchyn, 2014; Riccardi et al., 2006; Yan et al., 2013). Carbonates recrystallizing

365 during burial may also be prone to diagenetic modification of the $\delta^{34}S$ of CAS if the burial
366 fluids were sulfate rich (Fichtner et al., 2017, 2018; Present et al., 2015). The $\delta^{34}S$ in burial
367 fluids may be highly variable, and include sulfate from hydrocarbon or organic matter
368 degradation, dissolved evaporites, groundwater modified by MSR, or sulfate released by
369 dissolution of CAS (Dogramaci et al., 2001; Fichtner et al., 2018; Murray et al., 2020; Present
370 et al., 2019; Thode & Monster, 1965, 1970).

371 These diagenetic controls on the $\delta^{34}S$ of CAS decrease the precision and accuracy of the
372 proxy. This is quantified by its uncorrelated variance, which is much higher than that
373 observed in other seawater sulfate $\delta^{34}S$ proxies. Uncorrelated Paleozoic CAS data has a
374 standard deviation of 5.0‰, and that of Mesozoic CAS is 4.4‰, which is five to ten times
375 larger than that of Paleozoic and Mesozoic evaporites (1.0‰ and 0.4‰, respectively).
376 Further, diagenesis may have impacted accuracy by systematically biasing the $\delta^{34}S$ of CAS
377 with respect to the primary composition of seawater sulfate. For example, base level often
378 controls the stratigraphic arrangement of facies in carbonates successions, which can impart
379 biases as large as 10‰ on the $\delta^{34}S$ of CAS (Present et al., 2019; Richardson, Keating, et al.,
380 2019). Both the random and systematic variability is on the order of well-resolved rapid
381 changes of 3‰ to 6‰ in the $\delta^{34}S$ of marine barite and biogenic CAS.

382 3.2.4 Biogenic CAS

383 Biogenic CAS may offer a more robust $\delta^{34}S$ record than bulk CAS because biogenic
384 carbonate can often be readily separated from other limestone components, preservation
385 quality can be assessed, and vital effects appear to be small in most taxa (Kampschulte et al.,
386 2001; Paris, Fehrenbacher, et al., 2014; Present et al., 2015). In modern and cultured
387 biogenic carbonates, the incorporated sulfate has an isotopic composition within 2‰ of the
388 seawater from which it precipitated (Burdett et al., 1989; Kampschulte et al., 2001; Kaplan
389 et al., 1963; Mekhtiyeva, 1974; Paris et al., 2013; Paris, Fehrenbacher, et al., 2014; Present
390 et al., 2015). Recently, Rennie et al. (2018) produced a taxon-specific foraminiferal CAS
391 record with variance and secular trends comparable to the marine barite record.

392 Low-magnesium calcite, precipitated by many brachiopods, belemnites, and planktonic
393 foraminifera, is stable at Earth's surface and shallow burial conditions. The low-magnesium
394 calcite biogenic CAS $\delta^{34}S$ record has significantly improved the resolution of the
395 Phanerozoic $\delta^{34}S$ record during two key periods. First, during the Toarcian (Jurassic) Ocean
396 Anoxic Event, belemnite CAS displays a large (6‰) $\delta^{34}S$ excursion that is not well resolved
397 in the evaporite record (Gill, Lyons, & Jenkyns, 2011; Newton et al., 2011). Second, during
398 Carboniferous time, brachiopods record a prolonged recovery from a $\delta^{34}S$ maximum in
399 middle Devonian time (D. L. Johnson et al., 2020; Kampschulte et al., 2001; N. Wu et al.,
400 2014). However, aragonite and high-magnesium calcite, precipitated by many bivalves,
401 gastropods, corals, trilobites, echinoderms, bryozoans, and marine algae, dissolves and/or
402 recrystallizes much more readily than low-magnesium calcite (Brand & Veizer, 1980). Few
403 studies have investigated CAS $\delta^{34}S$ from formerly aragonitic fossils (Mekhtiyeva, 1974;
404 Present et al., 2015; Witts et al., 2018).

Unfortunately, well-preserved biogenic carbonate is rare in the rock record, especially during intervals of climatic or biologic crisis (e.g., mass extinction events). Even apparently well-preserved biogenic carbonate can still be susceptible to diagenetic alteration (Fichtner et al., 2018; Witts et al., 2018). Like the marine barite record, a significant expansion of the biogenic CAS $\delta^{34}S$ proxy record is limited by the availability of suitable sample material.

3.3 Discrepant early Phanerozoic proxy records

While all archives imperfectly estimate ancient seawater's composition, they provide generally indistinguishable estimates considering the sources of uncertainty discussed (Figure 2a). Paleozoic bulk rock CAS data, as a notable exception, commonly exhibit rapid $\delta^{34}S$ variability (Figure 1b), but other archives with less uncorrelated variance are absent or lack temporal resolution (Figure 1a). Throughout Phanerozoic strata, CAS data consistently display more unresolved variance than other archives, yet they record the same long-term trends (Figure 2), suggesting that some $\delta^{34}S$ excursions recorded by CAS may not represent changes in the composition of the ocean. The high uncorrelated variance in all early Paleozoic archives may mask $\delta^{34}S$ excursions on the order of those well-resolved in younger strata by all archives. Spatial and temporal variability in early Paleozoic CAS data may represent short residence times of sulfate in sulfidic oceans (e.g., Gill, Lyons, Young, et al., 2011; Kah et al., 2016), local diagenetic effects on the $\delta^{34}S$ of carbonate rocks (Present et al., 2015, 2019; Richardson, Keating, et al., 2019; Richardson, Newville, et al., 2019), or both (Edwards et al., 2019; Rose et al., 2019).

CAS $\delta^{34}S$ excursions often correlate with global perturbations evidenced by carbon isotope excursions and trace metal, pyrite sulfur isotope, and bioturbation intensity records (Canfield & Farquhar, 2009; Fike et al., 2015; Gill et al., 2007; Jones & Fike, 2013; Kah et al., 2016; Saltzman et al., 2015). Perhaps some CAS $\delta^{34}S$ excursions reflect widespread biogeochemical changes at the interface between pore fluid sulfur cycling and carbonate sediment diagenesis, including sulfate, dioxygen, and nutrient availability, organic productivity, or metabolic or oceanographic changes in carbonate mineral saturation (Rennie & Turchyn, 2014). Because part of the $\delta^{34}S$ variance in all archives derives from early diagenetic processes—such as MSR, pyrite formation, and sulfide reoxidation—consideration of these processes may reveal important temporal changes in carbon cycling in marine pore fluids (Present et al., 2019; Richardson, Keating, et al., 2019; N. Wu et al., 2010).

4 Conclusions

Phanerozoic $\delta^{34}S$ data were compiled from evaporites, barite, biogenic CAS, and bulk rock CAS and updated to a consistent time scale. The subset of seawater sulfate's $\delta^{34}S$ history possibly sampled by each proxy varied in space and time, and different suites of depositional and post-depositional processes added variance to each archive. The variance in each record increases with age, but the changing contribution of primary and secondary sources of variability over Phanerozoic time remains unclear.

Bulk CAS contains a statistically significant different distribution of $\delta^{34}S$ compositions than the biogenic CAS, evaporite, or barite records. Early diagenetic overprinting of CAS occurs in depositional environments where carbonate recrystallization and cementation coincides with sulfate-rich pore fluids with modified $\delta^{34}S$ values. Despite these complications, bulk CAS can be widely applied in ancient sedimentary basins and is the only archive readily able to resolve sulfur cycle changes during rapid biogeochemical events. Extending the breadth and resolution of the $\delta^{34}S$ record requires developing mechanistic understanding of how biogeochemical perturbations affect the marine diagenesis of carbonate rocks.

Acknowledgements

No new data were collected for this study. Datasets compiled for this research are tabulated in the Supplemental Material and referenced below. We thank Caltech DocuServe for obtaining many of the publications containing the compiled data, and John Grotzinger and Joe Kirschvink for thoughtful advising and feedback. Constructive reviews by Akshay Mehra and Julia Wilcots were greatly appreciated.

References

Adams, D. D., Hurtgen, M. T., & Sageman, B. B. (2010). Volcanic triggering of a biogeochemical cascade during Oceanic Anoxic Event 2. *Nature Geoscience*, *3*(3), 201–204. https://doi.org/10.1038/Ngeo743

Algeo, T. J., Henderson, C. M., Tong, J., Feng, Q., Yin, H., & Tyson, R. V. (2013). Plankton and productivity during the Permian–Triassic boundary crisis: An analysis of organic carbon fluxes. *Global and Planetary Change*, *105*, 52–67. https://doi.org/10.1016/j.gloplacha.2012.02.008

Arp, G., Ostertag-Henning, C., YÜCekent, S., Reitner, J., & Thiel, V. (2008). Methane-related microbial gypsum calcitization in stromatolites of a marine evaporative setting (Münder Formation, Upper Jurassic, Hils Syncline, north Germany). *Sedimentology*, *55*(5), 1227–1251. https://doi.org/10.1111/j.1365-3091.2007.00944.x

Ault, W. U., & Kulp, J. L. (1959). Isotopic geochemistry of sulphur. *Geochimica et Cosmochimica Acta*, *16*(4), 201–235. https://doi.org/10.1016/0016-7037(59)90112-7

Balderer, W., Pearson, F. J., & Soreau, S. (1991). Formation-Specific Characterization of Groundwaters. In F. J. Pearson, W. Balderer, H. H. Loosli, B. E. Lehmann, A. Matter, T. Peters, et al. (Eds.), *Applied Isotope Hydrogeology: A Case Study in Northern Switzerland: Technical Report 88-01* (pp. 297–374). Amsterdam: Elsevier. Retrieved from https://books.google.com/books?id=fEBs7PudzAEC

Baldermann, A., Deditius, A. P., Dietzel, M., Fichtner, V., Fischer, C., Hippler, D., et al. (2015). The role of bacterial sulfate reduction during dolomite precipitation: Implications from Upper Jurassic platform carbonates. *Chemical Geology*, *412*, 1–14. https://doi.org/10.1016/j.chemgeo.2015.07.020

Barkan, Y., Paris, G., Webb, S. M., Adkins, J. F., & Halevy, I. (2020). Sulfur isotope fractionation between aqueous and carbonate-associated sulfate in abiotic calcite and aragonite. *Geochimica et Cosmochimica Acta*. https://doi.org/10.1016/j.gca.2020.03.022

Ben-Yaakov, S. (1973). pH Buffering of Pore Water of Recent Anoxic Marine Sediments. *Limnology and Oceanography*, *18*(1), 86–94. https://doi.org/10.4319/lo.1973.18.1.0086

Berggren, W. A., Kent, D. V., Flynn, J. J., & Van Couvering, J. A. (1985). Cenozoic geochronology. *Geological Society of America Bulletin*, *96*, 1407–1418.

Berggren, W. A., Kent, D. V., Swisher, C. C., & Aubry, M.-P. (1995). A Revised Cenozoic Geochronology and Chronostratigraphy. In *Geochronology, Time Scales and Global Stratigraphic Correlation* (pp. 129–212). SEPM (Society for Sedimentary Geology). https://doi.org/10.2110/pec.95.04.0129

Bergström, S. M., Chen, X., Gutiérrez-Marco, J. C., & Dronov, A. (2009). The new chronostratigraphic classification of the Ordovician System and its relations to major regional series and stages and to δ13C chemostratigraphy. *Lethaia*, *42*(1), 97–107. https://doi.org/10.1111/j.1502-3931.2008.00136.x

Bernasconi, S. M., Meier, I., Wohlwend, S., Brack, P., Hochuli, P. A., Bläsi, H., et al. (2017). An evaporite-based high-resolution sulfur isotope record of Late Permian and Triassic seawater sulfate. *Geochimica et Cosmochimica Acta*, *204*, 331–349. https://doi.org/10.1016/j.gca.2017.01.047

Bishop, J. K. B. (1988). The barite-opal-organic carbon association in oceanic particulate matter. *Nature*, *332*(6162), 341–343. https://doi.org/10.1038/332341a0

Blomquist, P. K. (2016). Wolfcamp Horizontal Play, Midland Basin, West Texas, #10890 (2016). In *AAPG Pacific Section and Rocky Mountain Section Joint Meeting* (p. 34). Las Vegas, Nevada. Retrieved from http://www.searchanddiscovery.com/pdfz/documents/2016/10890blomquist/ndx_blomquist.pdf.html

Boschetti, T., Cortecchi, G., Toscani, L., & Iacumin, P. (2011). Sulfur and oxygen isotope compositions of Upper Triassic sulfates from Northerm Apennines (Italy): palaeogeographic and hidrogeochemical implications. *Geologica Acta*, *9*(2), 129–147. https://doi.org/10.1344/105.000001690

Bottrell, S. H., & Newton, R. J. (2006). Reconstruction of changes in global sulfur cycling from marine sulfate isotopes. *Earth-Science Reviews*, *75*(1–4), 59–83. https://doi.org/10.1016/j.earscirev.2005.10.004

Bowles, M. W., Mogollón, J. M., Kasten, S., Zabel, M., & Hinrichs, K.-U. (2014). Global rates of marine sulfate reduction and implications for sub–sea-floor metabolic activities. *Science*, *344*(6186), 889. https://doi.org/10.1126/science.1249213

Bowring, S. A., Erwin, D. H., Jin, Y. G., Martin, M. W., Davidek, K., & Wang, W. (1998). U/Pb Zircon Geochronology and Tempo of the End-Permian Mass Extinction. *Science*, *280*(5366), 1039–1045. https://doi.org/10.1126/science.280.5366.1039

Bradley, A. S., Leavitt, W. D., Schmidt, M., Knoll, A. H., Girguis, P. R., & Johnston, D. T. (2016). Patterns of sulfur isotope fractionation during microbial sulfate reduction. *Geobiology*, *14*(1), 91–101. https://doi.org/10.1111/gbi.12149

Brand, U., & Veizer, J. (1980). Chemical diagenesis of a multicomponent carbonate system; 1, Trace elements. *Journal of Sedimentary Research*, *50*(4), 1219–1236. https://doi.org/10.1306/212f7bb7-2b24-11d7-8648000102c1865d

526 Burdett, J. W., Arthur, M. A., & Richardson, M. (1989). A Neogene seawater sulfur isotope
527 age curve from calcareous pelagic microfossils. *Earth and Planetary Science Letters*, *94*,
528 189–198. https://doi.org/10.1016/0012-821x(89)90138-6
529 Burgess, S. D., Bowring, S., & Shen, S. (2014). High-precision timeline for Earth's most
530 severe extinction. *Proceedings of the National Academy of Sciences*.
531 https://doi.org/10.1073/pnas.1317692111
532 Burke, A., Present, T. M., Paris, G., Rae, E. C. M., Sandilands, B. H., Gaillardet, J., et al.
533 (2018). Sulfur isotopes in rivers: Insights into global weathering budgets, pyrite
534 oxidation, and the modern sulfur cycle. *Earth and Planetary Science Letters*.
535 https://doi.org/10.1016/j.epsl.2018.05.022
536 Buschendorf, Fr., Nielsen, H., Puchelt, H., & Ricke, W. (1963). Schwefel-Isotopen-
537 Untersuchungen am Pyrit-Sphalerit-Baryt-Lager Meggen/Lenne (Deutschland) und an
538 verschiedenen Devon-Evaporiten. *Geochimica et Cosmochimica Acta*, *27*(5), 501–523.
539 https://doi.org/10.1016/0016-7037(63)90085-1
540 Busenberg, E., & Plummer, N. L. (1985). Kinetic and thermodynamic factors controlling the
541 distribution of SO42− and Na+ in calcites and selected aragonites. *Geochimica et*
542 *Cosmochimica Acta*, *49*(3), 713–725. https://doi.org/10.1016/0016-7037(85)90166-8
543 Cai, C., Hu, W., & Worden, R. H. (2001). Thermochemical sulphate reduction in Cambro–
544 Ordovician carbonates in Central Tarim. *Marine and Petroleum Geology*, *18*(6), 729–
545 741. https://doi.org/10.1016/S0264-8172(01)00028-9
546 Canfield, D. E., & Farquhar, J. (2009). Animal evolution, bioturbation, and the sulfate
547 concentration of the oceans. *Proceedings of the National Academy of Sciences*, *106*(20),
548 8123–8127. https://doi.org/10.1073/pnas.0902037106
549 Chen, D., Wang, J., Racki, G., Li, H., Wang, C., Ma, X., & Whalen, M. T. (2013). Large
550 sulphur isotopic perturbations and oceanic changes during the Frasnian–Famennian
551 transition of the Late Devonian. *Journal of the Geological Society*, *170*(3), 465–476.
552 https://doi.org/10.1144/jgs2012-037
553 Chen, J., Zhao, R., Huo, W., Yao Yuyuan Pan, S., Shao, M., & Hai, C. (1981). Sulfur
554 Isotopes of Some Marine Gypsum. *Chinese Journal of Geology*, *3*, 009.
555 Chow, T. J., & Goldberg, E. D. (1960). On the marine geochemistry of barium. *Geochimica*
556 *et Cosmochimica Acta*, *20*(3), 192–198. https://doi.org/10.1016/0016-7037(60)90073-9
557 Church, T. M., & Wolgemuth, K. (1972). Marine barite saturation. *Earth and Planetary*
558 *Science Letters*, *15*(1), 35–44. https://doi.org/10.1016/0012-821X(72)90026-X
559 Claypool, G. E., Holser, W. T., Kaplan, I. R., Sakai, H., & Zak, I. (1980). The age curves of
560 sulfur and oxygen isotopes in marine sulfate and their mutual interpretation. *Chemical*
561 *Geology*, *28*, 199–260. https://doi.org/10.1016/0009-2541(80)90047-9
562 Cohen, K., Finney, S., Gibbard, P., & Fan, J.-X. (2013). The ICS international
563 chronostratigraphic chart. *Episodes*, *36*(3), 199–204.
564 Cortecci, G., Reyes, E., Berti, G., & Casati, P. (1981). Sulfur and oxygen isotopes in Italian
565 marine sulfates of Permian and Triassic ages. *Chemical Geology*, *34*(1), 65–79.
566 https://doi.org/10.1016/0009-2541(81)90072-3
567 Cramer, B. D., Loydell, D. K., Samtleben, C., Munnecke, A., Kaljo, D., Männik, P., et al.
568 (2010). Testing the limits of Paleozoic chronostratigraphic correlation via high-
569 resolution (<500 k.y.) integrated conodont, graptolite, and carbon isotope (δ13Ccarb)

biochemostratigraphy across the Llandovery–Wenlock (Silurian) boundary: Is a unified Phanerozoic time scale achievable? *Geological Society of America Bulletin*, 17.

Cramer, B. D., Condon, D. J., Söderlund, U., Marshall, C., Worton, G. J., Thomas, A. T., et al. (2012). U-Pb (zircon) age constraints on the timing and duration of Wenlock (Silurian) paleocommunity collapse and recovery during the "Big Crisis." *GSA Bulletin*, *124*(11–12), 1841–1857. https://doi.org/10.1130/B30642.1

Cressie, N., & Hawkins, D. M. (1980). Robust estimation of the variogram: I. *Journal of the International Association for Mathematical Geology*, *12*(2), 115–125. https://doi.org/10.1007/BF01035243

Dahl, T. W., Connelly, J. N., Li, D., Kouchinsky, A., Gill, B. C., Porter, S., et al. (2019). Atmosphere–ocean oxygen and productivity dynamics during early animal radiations. *Proceedings of the National Academy of Sciences*, *116*(39), 19352–19361. https://doi.org/10.1073/pnas.1901178116

Das, N., Horita, J., & Holland, H. D. (1990). Chemistry of fluid inclusions in halite from the Salina Group of the Michigan basin: Implications for Late Silurian seawater and the origin of sedimentary brines. *Geochimica et Cosmochimica Acta*, *54*(2), 319–327. https://doi.org/10.1016/0016-7037(90)90321-B

Davies, G. R., & Krouse, H. R. (1975). Sulphur isotope distribution in Paleozoic sulphate evaporites, Canadian Arctic Archipelago. *Geological Survey of Canada Paper*, *75–1 Part B*, 221–225.

Dogramaci, S. S., Herczeg, A. L., Schiff, S. L., & Bone, Y. (2001). Controls on δ34S and δ18O of dissolved sulfate in aquifers of the Murray Basin, Australia and their use as indicators of flow processes. *Applied Geochemistry*, *16*(4), 475–488. https://doi.org/10.1016/S0883-2927(00)00052-4

Edwards, C. T., Fike, D. A., Saltzman, M. R., Lu, W., & Lu, Z. (2018). Evidence for local and global redox conditions at an Early Ordovician (Tremadocian) mass extinction. *Earth and Planetary Science Letters*, *481*, 125–135. https://doi.org/10.1016/j.epsl.2017.10.002

Edwards, C. T., Fike, D. A., & Saltzman, M. R. (2019). Testing carbonate-associated sulfate (CAS) extraction methods for sulfur isotope stratigraphy: A case study of a Lower–Middle Ordovician carbonate succession, Shingle Pass, Nevada, USA. *Chemical Geology*, *529*, 119297. https://doi.org/10.1016/j.chemgeo.2019.119297

van Everdingen, R. O., Shakur, M. A., & Krouse, H. R. (1982). 34S and 18O abundances differentiate Upper Cambrian and Lower Devonian gypsum-bearing units, District of Mackenzie, N.W.T.—an update. *Canadian Journal of Earth Sciences*, *19*(6), 1246–1254. https://doi.org/10.1139/e82-106

Fanlo, I., & Ayora, C. (1998). The evolution of the Lorraine evaporite basin: implications for the chemical and isotope composition of the Triassic ocean. *Chemical Geology*, *146*(3), 135–154. https://doi.org/10.1016/S0009-2541(98)00007-2

Feely, H. W., & Kulp, J. L. (1957). Origin of Gulf Coast Salt-Dome Sulphur Deposits. *AAPG Bulletin*, *41*(8), 1802–1853.

Fichtner, V., Strauss, H., Immenhauser, A., Buhl, D., Neuser, R. D., & Niedermayr, A. (2017). Diagenesis of carbonate associated sulfate. *Chemical Geology*, *463*(Supplement C), 61–75. https://doi.org/10.1016/j.chemgeo.2017.05.008

Fichtner, V., Strauss, H., Mavromatis, V., Dietzel, M., Huthwelker, T., Borca, C. N., et al. (2018). Incorporation and subsequent diagenetic alteration of sulfur in Arctica islandica. *Chemical Geology*, *482*, 72–90. https://doi.org/10.1016/j.chemgeo.2018.01.035

Fike, D. A., & Grotzinger, J. P. (2008). A paired sulfate–pyrite δ34S approach to understanding the evolution of the Ediacaran–Cambrian sulfur cycle. *Geochimica et Cosmochimica Acta*, *72*(11), 2636–2648. https://doi.org/10.1016/j.gca.2008.03.021

Fike, D. A., & Grotzinger, J. P. (2010). A δ34SSO4 approach to reconstructing biogenic pyrite burial in carbonate-evaporite basins: An example from the Ara Group, Sultanate of Oman. *Geology*, *38*, 371–374.

Fike, D. A., Bradley, A. S., & Rose, C. V. (2015). Rethinking the Ancient Sulfur Cycle. *Annual Review of Earth and Planetary Sciences*, *43*(1), 593–622. https://doi.org/10.1146/annurev-earth-060313-054802

Fox, J. S., & Videtich, P. E. (1997). Revised estimate of δ34S for marine sulfates from the Upper Ordovician: data from the Williston Basin, North Dakota, U.S.A. *Applied Geochemistry*, *12*(1), 97–103. https://doi.org/10.1016/S0883-2927(96)00065-0

Froelich, P. N., Klinkhammer, G. P., Bender, M. L., Luedtke, N. A., Heath, G. R., Cullen, D., et al. (1979). Early oxidation of organic matter in pelagic sediments of the eastern equatorial Atlantic: suboxic diagenesis. *Geochimica et Cosmochimica Acta*, *43*, 1075–1090. https://doi.org/10.1016/0016-7037(79)90095-4

Gebbers, R. (2010). Geostatistics and Kriging. In M. H. Trauth, *MATLAB Recipes for Earth Sciences* (3rd Ed., pp. 235–254). Berlin, Germany: Springer-Verlag.

Gill, B. C., Lyons, T. W., & Saltzman, M. R. (2007). Parallel, high-resolution carbon and sulfur isotope records of the evolving Paleozoic marine sulfur reservoir. *Palaeogeography, Palaeoclimatology, Palaeoecology*, *256*, 156–173. https://doi.org/10.1016/j.palaeo.2007.02.030

Gill, B. C., Lyons, T. W., & Frank, T. D. (2008). Behavior of carbonate-associated sulfate during meteoric diagenesis and implications for the sulfur isotope paleoproxy. *Geochimica et Cosmochimica Acta*, *72*, 4699–4711. https://doi.org/10.1016/j.gca.2008.07.001

Gill, B. C., Lyons, T. W., & Jenkyns, H. C. (2011). A global perturbation to the sulfur cycle during the Toarcian Oceanic Anoxic Event. *Earth and Planetary Science Letters*, *312*, 484–496. https://doi.org/10.1016/j.epsl.2011.10.030

Gill, B. C., Lyons, T. W., Young, S. A., Kump, L. R., Knoll, A. H., & Saltzman, M. R. (2011). Geochemical evidence for widespread euxinia in the Later Cambrian ocean. *Nature*, *469*, 80–83.

Giri, S. J., & Swart, P. K. (2019). The influence of seawater chemistry on carbonate-associated sulfate derived from coral skeletons. *Palaeogeography, Palaeoclimatology, Palaeoecology*, *521*, 72–81. https://doi.org/10.1016/j.palaeo.2019.02.011

Gomes, M. L., Hurtgen, M. T., & Sageman, B. B. (2016). Biogeochemical sulfur cycling during Cretaceous oceanic anoxic events: A comparison of OAE1a and OAE2. *Paleoceanography*, *31*(2), 2015PA002869. https://doi.org/10.1002/2015PA002869

Gorjan, P., & Kaiho, K. (2007). Correlation and comparison of seawater δ34Ssulfate records at the Permian-Triassic transition. *Chemical Geology*, *243*, 275–285. https://doi.org/10.1016/j.chemgeo.2007.03.011

Grotzinger, J. P., & Kasting, J. F. (1993). New constraints on Precambrian ocean composition. *The Journal of Geology*, 235–243.

Guo, C., Chen, D., Song, Y., Zhou, X., Ding, Y., & Zhang, G. (2018). Depositional environments and cyclicity of the Early Ordovician carbonate ramp in the western Tarim Basin (NW China). *Journal of Asian Earth Sciences*, *158*, 29–48. https://doi.org/10.1016/j.jseaes.2018.02.006

Handford, C. R., & Dutton, S. P. (1980). Pennsylvanian–Early Permian Depositional Systems and Shelf-Margin Evolution, Palo Duro Basin, Texas. *AAPG Bulletin*, *64*(1), 88–106. https://doi.org/10.1306/2F918932-16CE-11D7-8645000102C1865D

Hannisdal, B., & Peters, S. E. (2011). Phanerozoic Earth System Evolution and Marine Biodiversity. *Science*, *334*(6059), 1121–1124. https://doi.org/10.1126/science.1210695

Hardie, L. A. (1984). Evaporites; marine or non-marine? *American Journal of Science*, *284*(3), 193–240. https://doi.org/10.2475/ajs.284.3.193

Harland, W., Armstrong, R., Cox, A., Craig, L., Smith, A., & Smith, D. (1990). *A Geologic Time Scale 1989*. Cambridge University Press.

Harrison, A. G., & Thode, H. G. (1958). Mechanism of the bacterial reduction of sulphate from isotope fractionation studies. *Transactions of the Faraday Society*, *54*, 84. https://doi.org/10.1039/tf9585400084

He, T., Zhu, M., Mills, B. J. W., Wynn, P. M., Zhuravlev, A. Y., Tostevin, R., et al. (2019). Possible links between extreme oxygen perturbations and the Cambrian radiation of animals. *Nature Geoscience*, 1. https://doi.org/10.1038/s41561-019-0357-z

Hearn, M. R., Machel, H. G., & Rostron, B. J. (2011). Hydrocarbon breaching of a regional aquitard: The Devonian Ireton Formation, Bashaw area, Alberta, Canada. *AAPG Bulletin*, *95*(6), 1009–1037. https://doi.org/10.1306/09271010050

Hitchon, B., & Krouse, H. R. (1972). Hydrogeochemistry of the surface waters of the Mackenzie River drainage basin, Canada—III. Stable isotopes of oxygen, carbon and sulphur. *Geochimica et Cosmochimica Acta*, *36*(12), 1337–1357. https://doi.org/10.1016/0016-7037(72)90066-X

Holland, H. D. (1973). Systematics of the isotopic composition of sulfur in the oceans during the Phanerozoic and its implications for atmospheric oxygen. *Geochimica et Cosmochimica Acta*, *37*(12), 2605–2616. https://doi.org/10.1016/0016-7037(73)90268-8

Holser, W. T. (1977). Catastrophic chemical events in the history of the ocean. *Nature*, *267*, 403–408.

Holser, W. T., & Kaplan, I. R. (1966). Isotope geochemistry of sedimentary sulfates. *Chemical Geology*, *1*, 93–135. https://doi.org/10.1016/0009-2541(66)90011-8

Holser, W. T., Maynard, J. B., & Cruikshank, K. (1989). Modelling the natural cycle of sulphur through Phanerozoic time. *Evolution of the Global Biogeochemical Sulphur Cycle. Wiley, New York*, 21–56.

Horacek, M., Brandner, R., Richoz, S., & Povoden-Karadeniz, E. (2010). Lower Triassic sulphur isotope curve of marine sulphates from the Dolomites, N-Italy. *Palaeogeography, Palaeoclimatology, Palaeoecology*, *290*(1), 65–70. https://doi.org/10.1016/j.palaeo.2010.02.016

Horner, T. J., Pryer, H. V., Nielsen, S. G., Crockford, P. W., Gauglitz, J. M., Wing, B. A., & Ricketts, R. D. (2017). Pelagic barite precipitation at micromolar ambient sulfate. *Nature Communications*, *8*(1), 1342. https://doi.org/10.1038/s41467-017-01229-5

Hovorka, S. D., Knauth, L. P., Fisher, R. S., & Gao, G. (1993). Marine to nonmarine facies transition in Permian evaporites of the Palo Duro Basin, Texas: Geochemical response. *GSA Bulletin*, *105*(8), 1119–1134. https://doi.org/10.1130/0016-7606(1993)105<1119:MTNFTI>2.3.CO;2

Hurtgen, M. T., Pruss, S. B., & Knoll, A. H. (2009). Evaluating the relationship between the carbon and sulfur cycles in the later Cambrian ocean: An example from the Port au Port Group, western Newfoundland, Canada. *Earth and Planetary Science Letters*, *281*(3–4), 288–297. https://doi.org/10.1016/j.epsl.2009.02.033

Insalaco, E., Virgone, A., Courme, B., Gaillot, J., Kamali, M., Moallemi, A., et al. (2006). Upper Dalan Member and Kangan Formation between the Zagros Mountains and offshore Fars, Iran: depositional system, biostratigraphy and stratigraphic architecture. *GeoArabia*, *11*(2), 75–176.

Jacquet, S. H. M., Henjes, J., Dehairs, F., Worobiec, A., Savoye, N., & Cardinal, D. (2007). Particulate Ba-barite and acantharians in the Southern Ocean during the European Iron Fertilization Experiment (EIFEX). *Journal of Geophysical Research: Biogeosciences*, *112*(G4). https://doi.org/10.1029/2006JG000394

John, E. H., Wignall, P. B., Newton, R. J., & Bottrell, S. H. (2010). δ34SCAS and δ18OCAS records during the Frasnian–Famennian (Late Devonian) transition and their bearing on mass extinction models. *Chemical Geology*, *275*(3–4), 221–234. https://doi.org/10.1016/j.chemgeo.2010.05.012

Johnson, C. A., Emsbo, P., Poole, F. G., & Rye, R. O. (2009). Sulfur- and oxygen-isotopes in sediment-hosted stratiform barite deposits. *Geochimica et Cosmochimica Acta*, *73*(1), 133–147. https://doi.org/10.1016/j.gca.2008.10.011

Johnson, D. L., Grossman, E. L., Webb, S. M., & Adkins, J. F. (2020). Brachiopod δ34SCAS microanalyses indicate a dynamic, climate-influenced Permo-Carboniferous sulfur cycle. *Earth and Planetary Science Letters*, *546*, 116428. https://doi.org/10.1016/j.epsl.2020.116428

Jones, D. S., & Fike, D. A. (2013). Dynamic sulfur and carbon cycling through the end-Ordovician extinction revealed by paired sulfate–pyrite δ34S. *Earth and Planetary Science Letters*, *363*, 144–155.

Jørgensen, B. B. (1982). Mineralization of organic matter in the sea bed- the role of sulphate reduction. *Nature*, *296*, 643–645.

Kah, L. C., Lyons, T. W., & Frank, T. D. (2004). Low marine sulphate and protracted oxygenation of the Proterozoic biosphere. *Nature*, *431*, 834–838.

Kah, L. C., Thompson, C. K., Henderson, M. A., & Zhan, R. (2016). Behavior of marine sulfur in the Ordovician. *Palaeogeography, Palaeoclimatology, Palaeoecology*, *458*, 133–153. https://doi.org/10.1016/j.palaeo.2015.12.028

Kaiho, K., Kajiwara, Y., Nakano, T., Miura, Y., Kawahata, H., Tazaki, K., et al. (2001). End-Permian catastrophe by a bolide impact: Evidence of a gigantic release of sulfur from the mantle. *Geology*, *29*, 815–818. https://doi.org/10.1130/0091-7613(2001)029<0815:epcbab>2.0.co;2

Kaiho, Kunio, Kajiwara, Y., Tazaki, K., Ueshima, M., Takeda, N., Kawahata, H., et al. (1999). Oceanic primary productivity and dissolved oxygen levels at the Cretaceous/Tertiary boundary: their decrease, subsequent warming, and recovery. *Paleoceanography*, *14*(4), 511–524.

Kaiho, Kunio, Kajiwara, Y., Chen, Z.-Q., & Gorjan, P. (2006). A sulfur isotope event at the end of the Permian. *Chemical Geology*, *235*(1–2), 33–47. https://doi.org/10.1016/j.chemgeo.2006.06.001

Kampschulte, A., & Strauss, H. (2004). The sulfur isotopic evolution of Phanerozoic seawater based on the analysis of structurally substituted sulfate in carbonates. *Chemical Geology*, *204*, 255–286. https://doi.org/10.1016/j.chemgeo.2003.11.013

Kampschulte, A., Bruckschen, P., & Strauss, H. (2001). The sulphur isotopic composition of trace sulphates in Carboniferous brachiopods: implications for coeval seawater, correlation with other geochemical cycles and isotope stratigraphy. *Chemical Geology*, *175*, 149–173. https://doi.org/10.1016/s0009-2541(00)00367-3

Kampschulte, Anke. (2001). *Schwefelisotopenuntersuchungen an strukturell substituierten Sulfaten in marinen Karbonaten des Phanerozoikums : Implikationen für die geochemische Evolution des Meerwassers und die Korrelation verschiedener Stoffkreisläufe*. Ruhr-Universität Bochum. Retrieved from http://www-brs.ub.ruhr-uni-bochum.de/netahtml/HSS/Diss/KampschulteAnke/

Kaplan, I. R., Emery, K. O., & Rittenberg, S. C. (1963). The distribution and isotopic abundance of sulphur in recent marine sediments off southern California. *Geochimica et Cosmochimica Acta*, *27*(4), 297–331. https://doi.org/10.1016/0016-7037(63)90074-7

Kaufmann, B. (2006). Calibrating the Devonian Time Scale: A synthesis of U–Pb ID–TIMS ages and conodont stratigraphy. *Earth-Science Reviews*, *76*(3–4), 175–190. https://doi.org/10.1016/j.earscirev.2006.01.001

Kendall, A. C., & Harwood, G. M. (1989). Shallow-Water Gypsum in the Castile Formation - Significance and Implications. In P. M. Harris & G. A. Grover (Eds.), *Subsurface and Outcrop Examination of the Capitan Shelf Margin, Northern Delaware Basin* (pp. 451–457). San Antonio, Texas: SEPM. Retrieved from https://pubs.geoscienceworld.org/books/book/1170/chapter/10575312/shallow-water-gypsum-in-the-castile-formation

Kerans, C., & Tinker, S. W. (1999). Extrinsic stratigraphic controls on development of the Capitan Reef Complex. In A. H. Saller, P. M. Harris, B. L. Kirkland, & S. J. Mazzullo (Eds.), *Geologic Framework of the Capitan Reef*. Tulsa, Oklahoma: SEPM (Society for Sedimentary Geology).

Kolonic, S., Wagner, T., Forster, A., Sinninghe Damsté, J. S., Walsworth-Bell, B., Erba, E., et al. (2005). Black shale deposition on the northwest African Shelf during the Cenomanian/Turonian oceanic anoxic event: Climate coupling and global organic carbon burial: BLACK SHALE DEPOSITION DURING THE CENOMA. *Paleoceanography*, *20*(1), n/a-n/a. https://doi.org/10.1029/2003PA000950

Korte, C., Kozur, H., Joachimski, M., Strauss, H., Veizer, J., & Schwark, L. (2004). Carbon, sulfur, oxygen and strontium isotope records, organic geochemistry and biostratigraphy across the Permian/Triassic boundary in Abadeh, Iran. *International Journal of Earth Sciences*, *93*(4), 565–581. https://doi.org/10.1007/s00531-004-0406-7

Kozik, N. P., Young, S. A., Bowman, C. N., Saltzman, M. R., & Them, T. R. (2019). Middle–Upper Ordovician (Darriwilian–Sandbian) paired carbon and sulfur isotope stratigraphy from the Appalachian Basin, USA: Implications for dynamic redox conditions spanning the peak of the Great Ordovician Biodiversification Event. *Palaeogeography, Palaeoclimatology, Palaeoecology*, *520*, 188–202. https://doi.org/10.1016/j.palaeo.2019.01.032

Kramm, U., & Wedepohl, K. H. (1991). The isotopic composition of strontium and sulfur in seawater of Late Permian (Zechstein) age. *Chemical Geology*, *90*(3), 253–262. https://doi.org/10.1016/0009-2541(91)90103-X

Kump, L. R., & Garrels, R. M. (1986). Modeling atmospheric O 2 in the global sedimentary redox cycle. *American Journal of Science*, *286*(5), 337–360. https://doi.org/10.2475/ajs.286.5.337

Kurtz, A. C., Kump, L. R., Arthur, M. A., Zachos, J. C., & Paytan, A. (2003). Early Cenozoic decoupling of the global carbon and sulfur cycles. *Paleoceanography*, *18*(4), 1090. https://doi.org/10.1029/2003PA000908

Lark, R. M., & Webster, R. (2006). Geostatistical mapping of geomorphic variables in the presence of trend. *Earth Surface Processes and Landforms*, *31*(7), 862–874. https://doi.org/10.1002/esp.1296

Li, P., Huang, J., Chen, M., & Bai, X. (2009). Coincident negative shifts in sulfur and carbon isotope compositions prior to the end-Permian mass extinction at Shangsi Section of Guangyuan, South China. *Frontiers of Earth Science in China*, *3*(1), 51–56. https://doi.org/10.1007/s11707-009-0018-4

Longinelli, A., & Flora, O. (2007). Isotopic composition of gypsum samples of Permian and Triassic age from the north-eastern Italian Alps: Palaeoenvironmental implications. *Chemical Geology*, *245*(3), 275–284. https://doi.org/10.1016/j.chemgeo.2007.08.009

Loprieno, A., Bousquet, R., Bucher, S., Ceriani, S., Dalla Torre, F. H., Fügenschuh, B., & Schmid, S. M. (2011). The Valais units in Savoy (France): a key area for understanding the palaeogeography and the tectonic evolution of the Western Alps. *International Journal of Earth Sciences*, *100*(5), 963–992. https://doi.org/10.1007/s00531-010-0595-1

Lowenstein, T. K., Hardie, L. A., Timofeeff, M. N., & Demicco, R. V. (2003). Secular variation in seawater chemistry and the origin of calcium chloride basinal brines. *Geology*, *31*(10), 857–860. https://doi.org/10.1130/G19728r.1

Loyd, S. J., Marenco, P. J., Hagadorn, J. W., Lyons, T. W., Kaufman, A. J., Sour-Tovar, F., & Corsetti, F. A. (2012). Sustained low marine sulfate concentrations from the Neoproterozoic to the Cambrian: Insights from carbonates of northwestern Mexico and eastern California. *Earth and Planetary Science Letters*, *339–340*(0), 79–94. https://doi.org/10.1016/j.epsl.2012.05.032

Lu, F. H., & Meyers, W. J. (2003). Sr, S, and OSO4 Isotopes and the Depositional Environments of the Upper Miocene Evaporites, Spain. *Journal of Sedimentary Research*, *73*(3), 444–450. https://doi.org/10.1306/093002730444

Luo, G., Kump, L. R., Wang, Y., Tong, J., Arthur, M. A., Yang, H., et al. (2010). Isotopic evidence for an anomalously low oceanic sulfate concentration following end-Permian mass extinction. *Earth and Planetary Science Letters*, *300*(1–2), 101–111. https://doi.org/10.1016/j.epsl.2010.09.041

Lyons, T. W., Walter, L. M., Gellatly, A. M., Martini, A. M., & Blake, R. E. (2004). Sites of anomalous organic remineralization in the carbonate sediments of South Florida, USA: The sulfur cycle and carbonate-associated sulfate. In J. P. Amend, K. J. Edwards, & T. W. Lyons (Eds.), *Sulfur Biogeochemistry - Past and Present* (pp. 161–176). Boulder, Colorado: Geological Society of America.

Lyu, Z., Zhang, L., Algeo, T. J., Zhao, L., Chen, Z.-Q., Li, C., et al. (2019). Global-ocean circulation changes during the Smithian–Spathian transition inferred from carbon-sulfur cycle records. *Earth-Science Reviews*. https://doi.org/10.1016/j.earscirev.2019.01.010

Maharjan, D., Jiang, G., Peng, Y., & Nicholl, M. J. (2018). Sulfur isotope change across the Early Mississippian K–O (Kinderhookian–Osagean) δ 13 C excursion. *Earth and Planetary Science Letters*, *494*, 202–215. https://doi.org/10.1016/j.epsl.2018.04.043

Marenco, P. J., Corsetti, F. A., Kaufman, A. J., & Bottjer, D. J. (2008). Environmental and diagenetic variations in carbonate associated sulfate: An investigation of CAS in the Lower Triassic of the western USA. *Geochimica et Cosmochimica Acta*, *72*, 1570–1582.

Marenco, P. J., Corsetti, F. A., Hammond, D. E., Kaufman, A. J., & Bottjer, D. J. (2008). Oxidation of pyrite during extraction of carbonate associated sulfate. *Chemical Geology*, *247*, 124–132.

Marenco, Pedro J., Marenco, K. N., Lubitz, R. L., & Niu, D. (2013). Contrasting long-term global and short-term local redox proxies during the Great Ordovician Biodiversification Event: A case study from Fossil Mountain, Utah, USA. *Palaeogeography, Palaeoclimatology, Palaeoecology*, *377*, 45–51. https://doi.org/10.1016/j.palaeo.2013.03.007

Marenco, Pedro J., Martin, K. R., Marenco, K. N., & Barber, D. C. (2016). Increasing global ocean oxygenation and the Ordovician Radiation: Insights from Th/U of carbonates from the Ordovician of western Utah. *Palaeogeography, Palaeoclimatology, Palaeoecology*, *458*, 77–84. https://doi.org/10.1016/j.palaeo.2016.05.014

Martin, E. E., & Scher, H. D. (2004). Preservation of seawater Sr and Nd isotopes in fossil fish teeth: bad news and good news. *Earth and Planetary Science Letters*, *220*(1), 25–39. https://doi.org/10.1016/S0012-821X(04)00030-5

Mazzullo, S. J. (1982). Stratigraphy and Depositional Mosaics of Lower Clear Fork and Wichita Groups (Permian), Northern Midland Basin, Texas. *AAPG Bulletin*, *66*(2), 210–227. https://doi.org/10.1306/03B59A67-16D1-11D7-8645000102C1865D

Mekhtiyeva, V. (1974). Sulfur isotopic composition of fossil molluscan shells as an indicator of hydrochemical conditions in ancient basins. *Geochemistry International*, *11*, 1188–1192.

Meng, F.-W., Zhang, Z., Yan, X., Ni, P., Liu, W.-H., Fan, F., & Xie, G.-W. (2019). Stromatolites in Middle Ordovician carbonate–evaporite sequences and their carbon and sulfur isotopes stratigraphy, Ordos Basin, northwestern China. *Carbonates and Evaporites*, *34*(1), 11–20. https://doi.org/10.1007/s13146-017-0367-0

Meng, F.-W., Zhang, Z., Schiffbauer, J. D., Zhuo, Q., Zhao, M., Ni, P., et al. (2019). The Yudomski event and subsequent decline: new evidence from δ34S data of lower and middle Cambrian evaporites in the Tarim Basin, western China. *Carbonates and Evaporites*, *34*(3), 1117–1129. https://doi.org/10.1007/s13146-017-0407-9

Meyers Stephen R., Sageman Bradley B., & Arthur Michael A. (2012). Obliquity forcing of organic matter accumulation during Oceanic Anoxic Event 2. *Paleoceanography*, *27*(3). https://doi.org/10.1029/2012PA002286

Mills, J. V., Gomes, M. L., Kristall, B., Sageman, B. B., Jacobson, A. D., & Hurtgen, M. T. (2017). Massive volcanism, evaporite deposition, and the chemical evolution of the Early Cretaceous ocean. *Geology*, *45*(5), 475–478. https://doi.org/10.1130/G38667.1

Murray, S. T., Higgins, J. A., Holmden, C., Lu, C., & Swart, P. K. (2020). Geochemical fingerprints of dolomitization in Bahamian carbonates: Evidence from sulphur, calcium, magnesium and clumped isotopes. *Sedimentology*. https://doi.org/10.1111/sed.12775

Newton, R. J., Pevitt, E. L., Wignall, P. B., & Bottrell, S. H. (2004). Large shifts in the isotopic composition of seawater sulphate across the Permo–Triassic boundary in northern Italy. *Earth and Planetary Science Letters*, *218*, 331–345. https://doi.org/10.1016/S0012-821X(03)00676-9

Newton, R. J., Reeves, E. P., Kafousia, N., Wignall, P. B., Bottrell, S. H., & Sha, J. (2011). Low marine sulfate concentrations and the isolation of the European epicontinental sea during the Early Jurassic. *Geology*, *39*, 7–10. https://doi.org/10.1130/g31326.1

Nielsen, H. (1989). Local and global aspects of the sulphur isotope age curve of oceanic sulphate. *Evolution of the Global Biogeochemical Sulphur Cycle. Wiley, New York*, 57–64.

Nielsen, H., & Ricke, W. (1964). Schwefel-isotopen verhältnisse von evaporiten aus deutschland; Ein beitrag zur kenntnis von δ34S im meerwasser-sulfat. *Geochimica et Cosmochimica Acta*, *28*(5), 577–591. https://doi.org/10.1016/0016-7037(64)90078-X

Novikov, D. A. (2017). Distribution of Cambrian salts in the western Siberian craton (Yurubcheno-Tokhomo field, Russia). *Arabian Journal of Geosciences*, *10*(1). https://doi.org/10.1007/s12517-016-2792-0

Ohkouchi, N., Kawamura, K., Kajiwara, Y., Wada, E., Okada, M., Kanamatsu, T., & Taira, A. (1999). Sulfur isotope records around Livello Bonarelli (northern Apennines, Italy) black shale at the Cenomanian-Turonian boundary. *Geology*, *27*, 535–538. https://doi.org/10.1130/0091-7613(1999)027<0535:siralb>2.3.co;2

Owens, J. D., Gill, B. C., Jenkyns, H. C., Bates, S. M., Severmann, S., Kuypers, M. M. M., et al. (2013). Sulfur isotopes track the global extent and dynamics of euxinia during Cretaceous Oceanic Anoxic Event 2. *Proceedings of the National Academy of Sciences*, *110*(46), 18407–18412. https://doi.org/10.1073/pnas.1305304110

Pankina, R. G., Maksimov, S. P., Kalinko, M. K., Monakhov, I. B., & Guriyeva, S. M. (1975). Sulfur isotopic composition in the Phanerozoic evaporites of Bulgaria. *Geochemistry International*, *12*(6), 79–83.

Paris, G., Sessions, A. L., Subhas, A. V., & Adkins, J. F. (2013). MC-ICP-MS measurement of δ34S and Δ33S in small amounts of dissolved sulfate. *Chemical Geology*, *345*, 50–61. https://doi.org/10.1016/j.chemgeo.2013.02.022

Paris, G., Fehrenbacher, J. S., Sessions, A. L., Spero, H. J., & Adkins, J. F. (2014). Experimental determination of carbonate-associated sulfate δ34S in planktonic foraminifera shells. *Geochemistry, Geophysics, Geosystems*, *15*(4), 1452–1461. https://doi.org/10.1002/2014GC005295

Paris, G., Adkins, J. F., Sessions, A. L., Webb, S. M., & Fischer, W. W. (2014). Neoarchean carbonate–associated sulfate records positive Δ33S anomalies. *Science*, *346*(6210), 739–741. https://doi.org/10.1126/science.1258211

Paytan, A., Kastner, M., Martin, E. E., Macdougall, J. D., & Herbert, T. (1993). Marine barite as a monitor of seawater strontium isotope composition. *Nature*, *366*, 445–449.

Paytan, A., Kastner, M., Campbell, D., & Thiemens, M. H. (1998). Sulfur Isotopic Composition of Cenozoic Seawater Sulfate. *Science*, *282*, 1459–1462. https://doi.org/10.1126/science.282.5393.1459

Paytan, A., Mearon, S., Cobb, K., & Kastner, M. (2002). Origin of marine barite deposits: Sr and S isotope characterization. *Geology*, *30*, 747–750. https://doi.org/10.1130/0091-7613(2002)030<0747:oombds>2.0.co;2

Paytan, A., Kastner, M., Campbell, D., & Thiemens, M. H. (2004). Seawater Sulfur Isotope Fluctuations in the Cretaceous. *Science*, *304*, 1663–1665. https://doi.org/10.1126/science.1095258

Peryt, T. M., Halas, S., & Hryniv, S. P. (2010). Sulphur and oxygen isotope signatures of late Permian Zechstein anhydrites, West Poland: seawater evolution and diagenetic constraints. *Geological Quarterly*, *54*, 387–400.

Pisarchik, Y. K., & Golubchina, M. N. (1975). On isotope ratios of sulfur in the Cambrian sulfatic limestones of the Siberian platform. *Geochemistry International*, *12*, 227–230.

Playà, E., Cendón, D. I., Travé, A., Chivas, A. R., & García, A. (2007). Non-marine evaporites with both inherited marine and continental signatures: The Gulf of Carpentaria, Australia, at ~70 ka. *Sedimentary Geology*, *201*(3–4), 267–285. https://doi.org/10.1016/j.sedgeo.2007.05.010

Pope, M. C., & Grotzinger, J. P. (2003). Paleoproterozoic Stark Formation, Athapuscow Basin, Northwest Canada: Record of Cratonic-Scale Salinity Crisis. *Journal of Sedimentary Research*, *73*(2), 280–295. https://doi.org/10.1306/091302730280

Posey, H. H., & Fisher, S. R. (1989). A sulfur and strontium isotopic investigation of Lower Permian anhydrite, Palo Duro Basin, Texas, U.S.A. *Applied Geochemistry*, *4*(4), 395–407. https://doi.org/10.1016/0883-2927(89)90015-2

Poulton, S. W., Henkel, S., März, C., Urquhart, H., Flögel, S., Kasten, S., et al. (2015). A continental-weathering control on orbitally driven redox-nutrient cycling during Cretaceous Oceanic Anoxic Event 2. *Geology*, *43*(11), 963–966. https://doi.org/10.1130/G36837.1

Present, T. M. (2018). *Controls on the Sulfur Isotopic Composition of Carbonate-Associated Sulfate* (Ph.D.). California Institute of Technology, Pasadena, California. Retrieved from http://resolver.caltech.edu/CaltechTHESIS:04042018-153105432

Present, T. M., Paris, G., Burke, A., Fischer, W. W., & Adkins, J. F. (2015). Large Carbonate Associated Sulfate isotopic variability between brachiopods, micrite, and other sedimentary components in Late Ordovician strata. *Earth and Planetary Science Letters*, *432*, 187–198. https://doi.org/10.1016/j.epsl.2015.10.005

Present, T. M., Gutierrez, M., Paris, G., Kerans, C., Grotzinger, J. P., & Adkins, J. F. (2019). Diagenetic controls on the isotopic composition of carbonate-associated sulphate in the Permian Capitan Reef Complex, West Texas. *Sedimentology*, *66*(7), 2605–2626. https://doi.org/10.1111/sed.12615

963 Prokoph, A., Shields, G. A., & Veizer, J. (2008). Compilation and time-series analysis of a
964 marine carbonate δ18O, δ13C, 87Sr/86Sr and δ34S database through Earth history.
965 *Earth-Science Reviews*, *87*(3–4), 113–133.
966 https://doi.org/10.1016/j.earscirev.2007.12.003
967 Qiu, Z., Sun, S., Wei, H., Wang, Q., Zou, C., & Zhang, Y. (2015). SIMS zircon U-Pb dating
968 from bentonites in the Penglaitan Global Stratotype Section for the Guadalupian–
969 Lopingian boundary (GLB), South China. *Geological Journal*.
970 Raab, M., & Spiro, B. (1991). Sulfur isotopic variations during seawater evaporation with
971 fractional crystallization. *Chemical Geology: Isotope Geoscience Section*, *86*(4), 323–
972 333. https://doi.org/10.1016/0168-9622(91)90014-N
973 Rennie, V. C. F., & Turchyn, A. V. (2014). The preservation of d34SSO4 and d18OSO4 in
974 carbonate-associated sulfate during marine diagenesis: A 25 Myr test case using marine
975 sediments. *Earth and Planetary Science Letters*, *395*, 13–23.
976 https://doi.org/10.1016/j.epsl.2014.03.025
977 Rennie, V. C. F., Paris, G., Sessions, A. L., Abramovich, S., Turchyn, A. V., & Adkins, J. F.
978 (2018). Cenozoic record of δ 34 S in foraminiferal calcite implies an early Eocene shift
979 to deep-ocean sulfide burial. *Nature Geoscience*, (11), 761–765.
980 https://doi.org/10.1038/s41561-018-0200-y
981 Riccardi, A. L., Arthur, M. A., & Kump, L. R. (2006). Sulfur isotopic evidence for
982 chemocline upward excursions during the end-Permian mass extinction. *Geochimica et*
983 *Cosmochimica Acta*, *70*, 5740–5752.
984 Richardson, J. A., Newville, M., Lanzirotti, A., Webb, S. M., Rose, C. V., Catalano, J. G., &
985 Fike, D. A. (2019). Depositional and diagenetic constraints on the abundance and spatial
986 variability of carbonate-associated sulfate. *Chemical Geology*, *523*, 59–72.
987 https://doi.org/10.1016/j.chemgeo.2019.05.036
988 Richardson, J. A., Keating, C., Lepland, A., Hints, O., Bradley, A. S., & Fike, D. A. (2019).
989 Silurian records of carbon and sulfur cycling from Estonia: The importance of
990 depositional environment on isotopic trends. *Earth and Planetary Science Letters*, *512*,
991 71–82. https://doi.org/10.1016/j.epsl.2019.01.055
992 Rine, M. J., Garrett, J. D., & Kaczmarek, S. E. (2017). A New Facies Architecture Model for
993 the Silurian Niagaran Pinnacle Reef Complexes of the Michigan Basin. In A. J. Macneil,
994 J. Lonnee, & R. Wood, *Characterization and Modeling of Carbonates–Mountjoy*
995 *Symposium 1*. SEPM (Society for Sedimentary Geology).
996 https://doi.org/10.2110/sepmsp.109.02
997 Rose, C. V., Fischer, W. W., Finnegan, S., & Fike, D. A. (2019). Records of carbon and
998 sulfur cycling during the Silurian Ireviken Event in Gotland, Sweden. *Geochimica et*
999 *Cosmochimica Acta*, *246*, 299–316. https://doi.org/10.1016/j.gca.2018.11.030
1000 Sakai, H. (1972). Oxygen isotopic ratios of some evaporites from Precambrian to Recent
1001 ages. *Earth and Planetary Science Letters*, *15*(2), 201–205.
1002 https://doi.org/10.1016/0012-821X(72)90061-1
1003 Saltzman, M. R., Cowan, C. A., Runkel, A. C., Runnegar, B., Stewart, M. C., & Palmer, A.
1004 R. (2004). The Late Cambrian Spice (δ13C) Event and the Sauk II-SAUK III Regression:
1005 New Evidence from Laurentian Basins in Utah, Iowa, and Newfoundland. *Journal of*
1006 *Sedimentary Research*, *74*(3), 366–377. https://doi.org/10.1306/120203740366

1007 Saltzman, M. R., Edwards, C. T., Adrain, J. M., & Westrop, S. R. (2015). Persistent oceanic
1008 anoxia and elevated extinction rates separate the Cambrian and Ordovician radiations.
1009 *Geology*, *43*(9), 807–810. https://doi.org/10.1130/g36814.1
1010 Schobben, M., Stebbins, A., Ghaderi, A., Strauss, H., Korn, D., & Korte, C. (2015).
1011 Flourishing ocean drives the end-Permian marine mass extinction. *Proceedings of the*
1012 *National Academy of Sciences*, *112*(33), 10298–10303.
1013 https://doi.org/10.1073/pnas.1503755112
1014 Schobben, M., Stebbins, A., Algeo, T. J., Strauss, H., Leda, L., Haas, J., et al. (2017). Volatile
1015 earliest Triassic sulfur cycle: A consequence of persistent low seawater sulfate
1016 concentrations and a high sulfur cycle turnover rate? *Palaeogeography,*
1017 *Palaeoclimatology, Palaeoecology*, *486*, 74–85.
1018 https://doi.org/10.1016/j.palaeo.2017.02.025
1019 Schrag, D. P., DePaolo, D. J., & Richter, F. M. (1995). Reconstructing past sea surface
1020 temperatures: Correcting for diagenesis of bulk marine carbonate. *Geochimica et*
1021 *Cosmochimica Acta*, *59*(11), 2265–2278. https://doi.org/10.1016/0016-7037(95)00105-
1022 9
1023 Schröder, S., Schreiber, B. C., Amthor, J. E., & Matter, A. (2004). Stratigraphy and
1024 environmental conditions of the terminal Neoproterozoic–Cambrian Period in Oman:
1025 evidence from sulphur isotopes. *Journal of the Geological Society*, *161*(3), 489–499.
1026 https://doi.org/10.1144/0016-764902-062
1027 Sim, M. S., Bosak, T., & Ono, S. (2011). Large Sulfur Isotope Fractionation Does Not
1028 Require Disproportionation. *Science*, *333*(6038), 74–77.
1029 https://doi.org/10.1126/science.1205103
1030 Sim, M. S., Ono, S., & Hurtgen, M. T. (2015). Sulfur isotope evidence for low and fluctuating
1031 sulfate levels in the Late Devonian ocean and the potential link with the mass extinction
1032 event. *Earth and Planetary Science Letters*, *419*, 52–62.
1033 https://doi.org/10.1016/j.epsl.2015.03.009
1034 Solomon, M., Rafter, T. A., & Dunham, K. C. (1971). Sulphur and oxygen isotope studies
1035 in the northern Pennines in relation to ore genesis. *Transactions of the Institution of*
1036 *Mining and Metallurgy Section B*, *80B*, 259–275.
1037 Song, H., Tong, J., Algeo, T. J., Song, H., Qiu, H., Zhu, Y., et al. (2014). Early Triassic
1038 seawater sulfate drawdown. *Geochimica et Cosmochimica Acta*, *128*(0), 95–113.
1039 https://doi.org/10.1016/j.gca.2013.12.009
1040 Song, H., Du, Y., Algeo, T. J., Tong, J., Owens, J. D., Song, H., et al. (2019). Cooling-driven
1041 oceanic anoxia across the Smithian/Spathian boundary (mid-Early Triassic). *Earth-*
1042 *Science Reviews*. https://doi.org/10.1016/j.earscirev.2019.01.009
1043 Spötl, C. (1988). Schwefelisotopendatierungen und fazielle Entwicklung permoskytischer
1044 Anhydrite in den Salzbergbauen von Dürrnberg/Hallstein und Hallstadt (Österreich).
1045 *Mitteilungen Der Gesellschaft Der Geologie- Und Bergbaustudenten in Österreich*, *34–*
1046 *35*, 209–229.
1047 Staudt, W. J., & Schoonen, M. A. A. (1995). Sulfate Incorporation into Sedimentary
1048 Carbonates. In *Geochemical Transformations of Sedimentary Sulfur* (Vol. 612, pp. 332–
1049 345). American Chemical Society. https://doi.org/10.1021/bk-1995-0612.ch018

1050 Stebbins, A., Algeo, T. J., Krystyn, L., Rowe, H., Brookfield, M., Williams, J., et al. (2019).
1051 Marine sulfur cycle evidence for upwelling and eutrophic stresses during Early Triassic
1052 cooling events. *Earth-Science Reviews*. https://doi.org/10.1016/j.earscirev.2018.09.007
1053 Stollhofen, H., Bachmann, G. H., Barnasch, J., Bayer, U., Beutler, G., Franz, M., et al.
1054 (2008). Upper Rotliegend to early cretaceous basin development. *Dynamics of Complex*
1055 *Intracontinental Basins. The Central European Basin System*, 181–210.
1056 Strauss, H. (1997). The isotopic composition of sedimentary sulfur through time.
1057 *Palaeogeography, Palaeoclimatology, Palaeoecology*, *132*, 97–118.
1058 https://doi.org/10.1016/s0031-0182(97)00067-9
1059 Taki, H. E., & Pratt, B. R. (2012). Syndepositional tectonic activity in an epicontinental basin
1060 revealed by deformation of subaqueous carbonate laminites and evaporites: Seismites in
1061 Red River strata (Upper Ordovician) of southern Saskatchewan, Canada. *Bulletin of*
1062 *Canadian Petroleum Geology*, *60*(1), 37–58. https://doi.org/10.2113/gscpgbull.60.1.37
1063 Theiling, B. P., & Coleman, M. (2015). Refining the extraction methodology of carbonate
1064 associated sulfate: Evidence from synthetic and natural carbonate samples. *Chemical*
1065 *Geology*, *411*, 36–48. https://doi.org/10.1016/j.chemgeo.2015.06.018
1066 Thode, H. G., & Monster, J. (1965). Sulfur-Isotope Geochemistry of Petroleum, Evaporites,
1067 and Ancient Seas. In A. Young & J. E. Galley (Eds.), *AAPG Memoir 4: Fluids in*
1068 *subsurface environments* (Vol. 71, pp. 367–377). Tulsa, Oklahoma: American
1069 Association of Petroleum Geologists. Retrieved from
1070 http://archives.datapages.com/data/specpubs/methodo2/data/a071/a071/0001/0350/036
1071 7.htm
1072 Thode, H. G., & Monster, J. (1970). Sulfur Isotope Abundances and Genetic Relations of Oil
1073 Accumulations in Middle East Basin. *AAPG Bulletin*, *54*(4), 627–637.
1074 Thode, H. G., Macnamara, J., & Fleming, W. H. (1953). Sulphur isotope fractionation in
1075 nature and geological and biological time scales. *Geochimica et Cosmochimica Acta*,
1076 *3*(5), 235–243. https://doi.org/10.1016/0016-7037(53)90042-8
1077 Thode, H. G., Monster, J., & Dunford, H. B. (1958). Sulphur Isotope Abundances in
1078 Petroleum and Associated Materials. *AAPG Bulletin*, *42*(11), 2619–2641.
1079 Thompson, Cara K., & Kah, L. C. (2012). Sulfur isotope evidence for widespread euxinia
1080 and a fluctuating oxycline in Early to Middle Ordovician greenhouse oceans.
1081 *Palaeogeography, Palaeoclimatology, Palaeoecology*, *313–314*(0), 189–214.
1082 https://doi.org/10.1016/j.palaeo.2011.10.020
1083 Thompson, Cara K., Kah, L. C., Astini, R., Bowring, S. A., & Buchwaldt, R. (2012).
1084 Bentonite geochronology, marine geochemistry, and the Great Ordovician
1085 Biodiversification Event (GOBE). *Palaeogeography, Palaeoclimatology,*
1086 *Palaeoecology*, *321–322*(0), 88–101. https://doi.org/10.1016/j.palaeo.2012.01.022
1087 Thompson, Cara Kim. (2011). *Carbon and Sulfur Cycling in Early Paleozoic Oceans* (Ph.D.
1088 diss). University of Tennessee, Knoxville.
1089 Toggweiler, J. R., & Sarmiento, J. L. (1985). Glacial to Interglacial Changes in Atmospheric
1090 Carbon Dioxide: The Critical Role of Ocean Surface Water in High Latitudes. In *The*
1091 *Carbon Cycle and Atmospheric CO2: Natural Variations Archean to Present* (pp. 163–
1092 184). American Geophysical Union (AGU). https://doi.org/10.1029/GM032p0163

Torres, M. A., West, A. J., & Li, G. (2014). Sulphide oxidation and carbonate dissolution as a source of CO_2 over geological timescales. *Nature*, *507*(7492), 346–349. https://doi.org/10.1038/nature13030

Torres, M. E., Brumsack, H. J., Bohrmann, G., & Emeis, K. C. (1996). Barite fronts in continental margin sediments: a new look at barium remobilization in the zone of sulfate reduction and formation of heavy barites in diagenetic fronts. *Chemical Geology*, *127*, 125–139. https://doi.org/10.1016/0009-2541(95)00090-9

Turchyn, A. V., & DePaolo, D. J. (2019). Seawater Chemistry Through Phanerozoic Time. *Annual Review of Earth and Planetary Sciences*, *47*(1), 197–224. https://doi.org/10.1146/annurev-earth-082517-010305

Turchyn, A. V., Schrag, D. P., Coccioni, R., & Montanari, A. (2009). Stable isotope analysis of the Cretaceous sulfur cycle. *Earth and Planetary Science Letters*, *285*, 115–123. https://doi.org/10.1016/j.epsl.2009.06.002

Utrilla, R., Pierre, C., Orti, F., & Pueyo, J. J. (1992). Oxygen and sulphur isotope compositions as indicators of the origin of Mesozoic and Cenozoic evaporites from Spain. *Chemical Geology*, *102*(1), 229–244. https://doi.org/10.1016/0009-2541(92)90158-2

Veizer, J., Holser, W. T., & Wilgus, C. K. (1980). Correlation of 13C12C and 34S32S secular variations. *Geochimica et Cosmochimica Acta*, *44*(4), 579–587. https://doi.org/10.1016/0016-7037(80)90250-1

Vinogradov, V. I. (2007). Was there a conflict at the Neoproterozoic-Cambrian boundary: Evidence from sulfur isotope composition? *Lithology and Mineral Resources*, *42*(1), 1–14. https://doi.org/10.1134/S0024490207010014

Voigt, S., Erbacher, J., Mutterlose, J., Weiss, W., Westerhold, T., Wiese, F., et al. (2008). The Cenomanian – Turonian of the Wunstorf section – (North Germany): global stratigraphic reference section and new orbital time scale for Oceanic Anoxic Event 2. *Newsletters on Stratigraphy*, *43*(1), 65–89. https://doi.org/10.1127/0078-0421/2008/0043-0065

Vredenburgh, L. D., & Cheney, E. S. (1971). Sulfur and carbon isotopic investigation of petroleum, Wind River basin, Wyoming. *AAPG Bulletin*, *55*(11), 1954–1975.

Walker, J. C. (1986). Global geochemical cycles of carbon, sulfur and oxygen. *Marine Geology*, *70*(1), 159–174.

Warren, J. K. (2010). Evaporites through time: Tectonic, climatic and eustatic controls in marine and nonmarine deposits. *Earth-Science Reviews*, *98*(3), 217–268. https://doi.org/10.1016/j.earscirev.2009.11.004

Webster, R., & Oliver, M. A. (2007). *Geostatistics for environmental scientists* (2nd ed.). Chichester, UK: Wiley.

Wei, W., & Gartner, S. (1993). 2. Neogene Calcareous Nannofossils from Sites 811 and 819 Through 825, offshore Northeastern Australia. In J. A. McKenzie, P. J. Davies, & A. Palmer-Julson (Eds.), *Scientific Results* (Vol. 133, pp. 19–37). College Station, Texas: Ocean Drilling Program. https://doi.org/10.2973/odp.proc.sr.133.1993

Westerhold, T., Röhl, U., Raffi, I., Fornaciari, E., Monechi, S., Reale, V., et al. (2008). Astronomical calibration of the Paleocene time. *Palaeogeography, Palaeoclimatology, Palaeoecology*, *257*(4), 377–403. https://doi.org/10.1016/j.palaeo.2007.09.016

Witts, J. D., Newton, R. J., Mills, B. J. W., Wignall, P. B., Bottrell, S. H., Hall, J. L. O., et al. (2018). The impact of the Cretaceous–Paleogene (K–Pg) mass extinction event on the global sulfur cycle: Evidence from Seymour Island, Antarctica. *Geochimica et Cosmochimica Acta*. https://doi.org/10.1016/j.gca.2018.02.037

Worden, R. H., Smalley, P. C., & Fallick, A. E. (1997). Sulfur cycle in buried evaporites. *Geology*, *25*(7), 643–646. https://doi.org/10.1130/0091-7613(1997)025<0643:SCIBE>2.3.CO;2

Wotte, T., Strauss, H., & Sundberg, F. A. (2011). Carbon and Sulfur Isotopes from the Cambrian Series 2-Cambrian Series 3 of Laurentia and Siberia. In J. S. Hollingsworth, F. A. Sundberg, & J. R. Foster (Eds.), *Museum of Northern Arizona Bulletin 67: Cambrian Stratigraphy and Paleontology of Northern Arizona and Southern Nevada: The 16th Field Conference of the Cambrian Stage Subdivision Working Group, International Subcommission on Cambrian Stratigraphy, Flagstaff, Arizona, and Southern Nevada, United States* (pp. 43–63). Flagstaff, Arizona: Museum of Northern Arizona.

Wotte, T., Shields-Zhou, G. A., & Strauss, H. (2012). Carbonate-associated sulfate: Experimental comparisons of common extraction methods and recommendations toward a standard analytical protocol. *Chemical Geology*, *326–327*, 132–144. https://doi.org/10.1016/j.chemgeo.2012.07.020

Wright, J. D., & Kroon, D. (2000). Planktonic foraminiferal biostratigraphy of Leg 166. In P. K. Swart, G. P. Eberli, M. J. Malone, & J. F. Sarg (Eds.), *Scientific Results* (Vol. 166, pp. 3–12). College Station, Texas: Ocean Drilling Program. https://doi.org/10.2973/odp.proc.sr.166.2000

Wu, N. (2013). *Sulfur isotopic evolution of Phanerozoic and Ediacaran seawater sulfate*. University of Maryland, College Park, Md. Retrieved from http://hdl.handle.net/1903/14016

Wu, N., Farquhar, J., Strauss, H., Kim, S.-T., & Canfield, D. E. (2010). Evaluating the S-isotope fractionation associated with Phanerozoic pyrite burial. *Geochimica et Cosmochimica Acta*, *74*(7), 2053–2071. https://doi.org/10.1016/j.gca.2009.12.012

Wu, N., Farquhar, J., & Strauss, H. (2014). δ34S and Δ33S records of Paleozoic seawater sulfate based on the analysis of carbonate associated sulfate. *Earth and Planetary Science Letters*, *399*(0), 44–51. https://doi.org/10.1016/j.epsl.2014.05.004

Wu, Q., Ramezani, J., Zhang, H., Yuan, D., Erwin, D. H., Henderson, C. M., et al. (2020). High-precision U-Pb zircon age constraints on the Guadalupian in West Texas, USA. *Palaeogeography, Palaeoclimatology, Palaeoecology*, *548*, 109668. https://doi.org/10.1016/j.palaeo.2020.109668

Yadong, S., Xulong, L., Haishui, J., Genming, L., Si, S., Chunbo, Y., & Wignall, P. B. (2008). Guadalupian (Middle Permian) Conodont Faunas at Shangsi Section, Northeast Sichuan Province. *Journal of China University of Geosciences*, *19*(5), 451–460. https://doi.org/10.1016/S1002-0705(08)60050-3

Yan, D., Zhang, L., & Qiu, Z. (2013). Carbon and sulfur isotopic fluctuations associated with the end-Guadalupian mass extinction in South China. *Gondwana Research*, *24*(3–4), 1276–1282. https://doi.org/10.1016/j.gr.2013.02.008

Yang, C., Li, X.-H., Zhu, M., Condon, D. J., & Chen, J. (2018). Geochronological constraint on the Cambrian Chengjiang biota, South China. *Journal of the Geological Society*, *175*(4), 659–666. https://doi.org/10.1144/jgs2017-103

Yao, W., Paytan, A., & Wortmann, U. G. (2018). Large-scale ocean deoxygenation during the Paleocene-Eocene Thermal Maximum. *Science*, *361*(6404), 804–806. https://doi.org/10.1126/science.aar8658

Yao, W., Paytan, A., Griffith, E. M., Martínez-Ruiz, F., Markovic, S., & Wortmann, U. G. (2020). A revised seawater sulfate S-isotope curve for the Eocene. *Chemical Geology*, *532*, 119382. https://doi.org/10.1016/j.chemgeo.2019.119382

Yeremenko, N. A., & Pankina, R. G. (1972). Variations of 34S in Sulfates of Recent and Ancient Marine Basins of the Soviet Union. *Geochemistry International*, *10*, 45–54.

Young, S. A., Gill, B. C., Edwards, C. T., Saltzman, M. R., & Leslie, S. A. (2016). Middle–Late Ordovician (Darriwilian–Sandbian) decoupling of global sulfur and carbon cycles: Isotopic evidence from eastern and southern Laurentia. *Palaeogeography, Palaeoclimatology, Palaeoecology*, *458*, 118–132. https://doi.org/10.1016/j.palaeo.2015.09.040

Young, S. A., Kleinberg, A., & Owens, J. D. (2019). Geochemical evidence for expansion of marine euxinia during an early Silurian (Llandovery–Wenlock boundary) mass extinction. *Earth and Planetary Science Letters*, *513*, 187–196. https://doi.org/10.1016/j.epsl.2019.02.023

Zhang, L., Zhao, L., Chen, Z.-Q., Algeo, T. J., Li, Y., & Cao, L. (2015). Amelioration of marine environments at the Smithian–Spathian boundary, Early Triassic. *Biogeosciences*, *12*(5), 1597–1613.

Zhu, M., Yang, A., Yuan, J., Li, G., Zhang, J., Zhao, F., et al. (2019). Cambrian integrative stratigraphy and timescale of China. *Science China Earth Sciences*, *62*(1), 25–60. https://doi.org/10.1007/s11430-017-9291-0